Study of Majorana Fermions in Topological Superconductors and Vortex States Through Numerically Efficient Algorithms

A Thesis Submitted to the
College of Graduate Studies and Research
in Partial Fulfillment of the Requirements
for the degree of Master of Science
in the Department of Physics and Engineering Physics
University of Saskatchewan
Saskatoon

By
Evan D. B. Smith

Permission to Use

In presenting this thesis in partial fulfilment of the requirements for a Postgraduate degree from the University of Saskatchewan, I agree that the Libraries of this University may make it freely available for inspection. I further agree that permission for copying of this thesis in any manner, in whole or in part, for scholarly purposes may be granted by the professor or professors who supervised my thesis work or, in their absence, by the Head of the Department or the Dean of the College in which my thesis work was done. It is understood that any copying or publication or use of this thesis or parts thereof for financial gain shall not be allowed without my written permission. It is also understood that due recognition shall be given to me and to the University of Saskatchewan in any scholarly use which may be made of any material in my thesis.

Requests for permission to copy or to make other use of material in this thesis in whole or part should be addressed to:

Head of the Department of Physics and Engineering Physics
116 Science Place
University of Saskatchewan
Saskaton, Saskatchewan
Canada
S7N 5E2

Abstract

Recent developments in the study of Majorana fermions through braid theory have shown that there exists a set of interchanges that allow for the realization of true quantum computation. Alongside these developments there have been studies of topological superconductivity which show the existence of states that exhibit non-Abelian exchange statistics. Motivated by these developments we study the differences between Abelian and non-Abelian topological phase in the vortex state through the Bogoliubov de-Gennes (BdG) formalism.

Due to our interests in low-energy states we first implement computationally efficient algorithms for calculating the mean fields and computing eigenpairs in an arbitrary energy window. We have shown that these algorithms adequately reproduce results obtained from a variety of other techniques and show that these algorithms retain spatial inhomogeneity information. Our results show topological superconductivity and vortex states can coexist; providing a means to realize zero-energy bound states, the number of which corresponds to the topological phase. With the use of our methods we present results contrasting the differences between Abelian and non-Abelian topological phase.

Our calculations show that an increase in Zeeman field affects numerous parameters within topological superconductors. It causes the order parameter to become more sensitive to temperature variations in addition to a reduced rate of recovery to the bulk value from a vortex core. The increased field suppresses spin-up local density of states (LDOS) in close proximity to the vortex core for low-energy states. Further, it narrows the spectral gap at the lattice centre. Both energy spectrum and LDOS calculations confirm that trivial topological phase have no zero-energy bound states, Abelian phases have an even number, while non-Abelian phases have an odd number.

Acknowledgements

First and foremost, I would like to express my sincerest gratitude to Professor Kaori Tanaka for her continuous involvement in my studies. She has provided unprecedented motivation, support, and leadership, and contributed her vast knowledge to further my own. Without her my growth as a physicist, and more importantly as an individual, would have been significantly hindered.

Secondly, I thank all other members of my committee: Professor John Tse, Professor Rainer Dick, and Professor Glenn Hussey. Their collective comments provided nescessary motivation to broaden my knowledge and understanding of my research from different perspectives.

Dr. Nagai has graciously offered his extensive knowledge and experience through sharing notes, doccuments, and software in effort to further my understanding in this exciting field of research. For all of this and so much more I would like to express my most sincere and heartfelt gratitude to Dr. Yuki Nagai at the Japan Atomic Energy Agency.

I would like to express my thanks to the numerous personnel associated with Compute Canada, WestGrid, and the high-performance computing facilities at the University of Saskatchewan for their devotion and assistance in teaching high-performance computing architectures and paradigms. The resources that I have graciously been given access to provide the nescessary computational power to carry out my research.

Last but not least, I would like to thank my fellow research group members. I can not adequatley express my gratitude for the countless stimulating discussions, frusturating troubleshooting, and unwavering friendship in the past years.

Dedicated to everyone who never gave up on me, even when I wanted nothing more than to give up on myself.

Contents

List of Tables

List of Figures

List of Abbreviations

BCS	Bardeen-Cooper-Schrieffer
BdG	Bogoliubov de-Gennes'
CKPE	Chebyshev Kernel Polynomial Expansion
SS	Sakurai-Sugiura
DD	Direct Diagonalization
RAM	Random Access Memory
OMP	Open Multi-Processing
MPI	Message Passing Interface
TSC	Topological Superconductivity
LDOS	Local Density of States

Chapter 1

Introduction

1.1 Motivation

The phenomena of superconductivity was first discovered over one hundred years ago by Dutch physicist Heike Kamerlingh Onnes by pure coincidence during his quest to liquefy helium [24]. During testing he noted that the electrical resistivity of a sample of pure mercury abruptly dropped to unmeasurable values (below 10^{-6} Ω) at a temperature of around 4 K. This accidental discovery has since sparked tremendous amounts of research in the field of materials science and thus lead to numerous subsequent discoveries; many of which hold promise in future technological applications. Today's age sees new materials being developed on a continual basis. Several materials are known to exhibit superconducting properties well above 77 K; a temperature that is easily attainable via liquid nitrogen cooling. As of 2014, $HgBa_2Ca_2Cu_3O_8$ has the highest recorded transition temperature of around 133 K, albeit under highly controlled laboratory settings [1].

In the ongoing quest to find room-temperature superconductors [2] new kinds of superconducting materials keep emerging. The discovery of a family of novel materials called topological insulators and the subsequent discovery of topological superconductivity have since opened an exciting new field of research in condensed matter physics and materials science. One feature of topological superconductivity that makes this field significant is the possible existence of Majorana fermions as elementary excitations. Majorana fermions, which are its own antiparticle and obey non-Abelian exchange statistics, may well play a pivotal role in unlocking the vast potential of quantum computation. Although Majorana fermions were first hypothesized by Italian physicist Ettore Majorana in 1937 [26], it was not until late 2014 that they were experimentally observed [8].

1.2 Classification of Superconductors

There are two fundamentally different types of superconductors, type I and type II [1]. A material must satisfy two basic criteria to be classified as a superconductor. It must possess zero electrical resistance at zero temperature, but more importantly it must exhibit the so-called Meissner effect; the rejection of an external magnetic field from the materials interior. All superconductors have two characteristic length scales; the penetration depth λ and the coherence length ξ. Within the macroscopic Ginzburg-Landau theory of superconductivity the coherence length ξ represents the size of a Cooper pair [3]. Whereas λ represents the distance an external magnetic field penetrates into the material. The ratio between these two parameters dictates how the superconductor is classified according to

$$\frac{\lambda}{\xi} \in \begin{cases} [0, \frac{1}{\sqrt{2}}] & \text{Type I} \\ (\frac{1}{\sqrt{2}}, \infty) & \text{Type II} \end{cases}. \tag{1.1}$$

Superconductors are characterized by a external magnetic field versus temperature curve, or more generally by a magnetic field-temperature-pressure surface. Any combination of conditions above this surface results in a non-superconducting state while any combination below this surface results in a superconducting state. As a result of these characteristics this surface is known as the transitional surface. Examples of this surface at a fixed pressure are shown in Figs. 1.1 and 1.2.

[1] Technically there are three unique types. In addition to type I and II, there exists a "type 1.5" superconductor. This third classification is unique in the sense that if a material is composed of two bands it will have two different superconducting length scales given by ξ_1 and ξ_2. The material is a type 1.5 superconductor if one of the length scales would classify the material as type I while the other would classify it as type II [5]. Understandably, type 1.5 superconductors have some properties of both the other classifications. For simplicity we discuss only type I and II here.

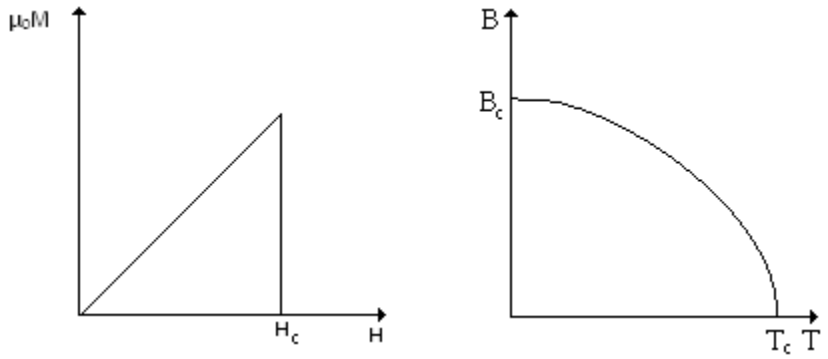

Figure 1.1: Type I superconducting transition surface at a fixed pressure.

The right portion of Fig. 1.1 depicts a typical magnetic field-temperature surface of a type I superconductor. The material acts as a pure superconductor when the applied external magnetic field is less than the critical value, H_c, for a given temperature below the critical temperature, T_c. The left portion depicts the Meissner effect. The demagnetization coefficient increases linearly with respect to the externally applied magnetic field resulting in zero net internal magnetic field. This trend continues until the external magnetic field is greater than the critical value which causes the superconducting state to be broken leaving the material to act as a normal conductor.

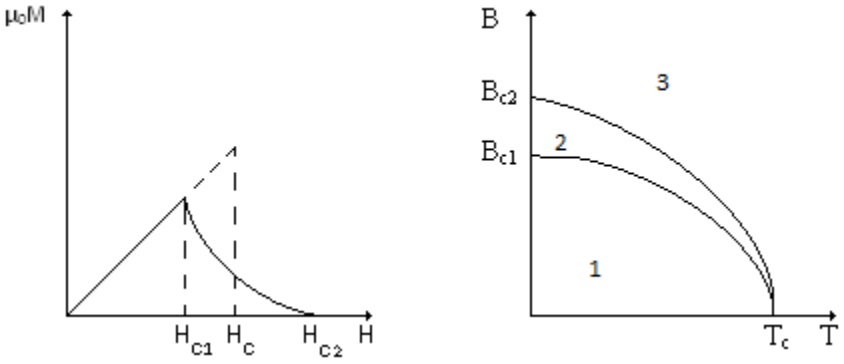

Figure 1.2: Type II superconducting transition surface at a fixed pressure.

The right portion of Fig. 1.2 depicts a typical magnetic field-temperature surface of a type II superconductor. Similar to type I, when the material is subject to any set of conditions in the first region the material acts as a pure superconductor. Any set of conditions in region three causes the material to act as a strictly non-superconducting material. The left

image indicates the material acts as a type I superconductor up until H_{c1} and as a normal conductor after H_{c2}. The region between H_{c1} and H_{c2} corresponds to region two on the right image and is commonly referred to as the mixed state. This mixed states allows for the penetration of some but not all magnetic field lines. The result is a material that consists of some superconducting and some non-superconducting regions.

1.3 Conventional BCS Theory

Although the London Equations were originally formulated in 1935 it was not until 1948 where Fritz London postulated that his and his brother's equations are a manifestation of coherent states within superconducting bodies [11]. This postulation provided the necessary momentum for the scientific community to continue investigations into the microscopic theory of superconducting phenomena. Cooper's calculations of electron pairs interacting with an attractive potential in addition to collaborations with Bardeen and Schrieffer lead to the first microscopic theory of superconductivity. The derivation of the Bardeen-Cooper-Schrieffer (BCS) theory [3] begins with a reduced model Hamiltonian

$$H_{reduced} = \sum_{k} \sum_{s} \epsilon_k n_{k,s} + \sum_{k} \sum_{k'} V_{k,k'} b^{\dagger}_{k'} b_k, \tag{1.2}$$

where k is the wavenumber, and s is a spin label. The creation and annihilation operators for Cooper pairs, $b^{\dagger}_{k'}$ and b_k, respectively, are simply products of electron creation and annihilation operators:

$$\begin{aligned} b^{\dagger}_{k'} &= c^{\dagger}_{k',\uparrow} c^{\dagger}_{-k',\downarrow} \\ b_k &= c_{-k,\downarrow} c_{k,\uparrow}. \end{aligned} \tag{1.3}$$

Cooper found that electrons pair such that their wavevectors k and $\bar{k}$ satisfy $|k| = |\bar{k}|$. One possible solution is $k = -\bar{k}$. In accordance with the Fermi-Dirac statistics one electron in the pair is spin up denoted by $\uparrow$ whereas the other is spin down denoted by $\downarrow$. The pairing of electrons into an aptly named Cooper pair is due to a net attractive interaction between the electrons composing the pair. The net attractive potential arises as a result of ions within

the bulk of the superconducting material screening the Coulomb interactions between the electrons. Cooper found that under any magnitude of net attractive potential between two electrons a bound state will be formed. Namely, Cooper pair formation is a result of pairing potential, $V_{k,k'}$, being negative around the Fermi surface.

If we expand our model Hamiltonian to explicitly account for the spin degree of freedom we find

$$H_{reduced} = \sum_{k} \epsilon_k(\hat{n}_{k,\uparrow} + \hat{n}_{-k,\downarrow}) + \sum_{k}\sum_{k'} V_{k,k'} b^{\dagger}_{k'} b_k, \tag{1.4}$$

where the term $\hat{n}_{k,\uparrow}$ is the occupation number for electrons with wavenumber k and spin up, and the term $\hat{n}_{-k,\downarrow}$ is the occupation number for electrons with wavenumber $-k$ and spin down. The number operators are described by the following relations:

$$\begin{aligned} \hat{n}_{k,\uparrow} &= c^{\dagger}_{k,\uparrow} c_{k,\uparrow} \\ \hat{n}_{-k,\downarrow} &= c^{\dagger}_{-k,\downarrow} c_{-k,\downarrow}. \end{aligned} \tag{1.5}$$

The next step of the derivation requires us to manipulate $\hat{n}_{k,\uparrow}+\hat{n}_{-k,\downarrow}$ into a form that contains only Cooper pair operators. This begins by writing them in terms of electron operators and inserting unity between terms:

$$\begin{aligned} \hat{n}_{k,\uparrow} + \hat{n}_{-k,\downarrow} &= c^{\dagger}_{k,\uparrow} c_{k,\uparrow} + c^{\dagger}_{-k,\downarrow} c_{-k,\downarrow} \\ &= c^{\dagger}_{k,\uparrow} c^{\dagger}_{-k,\downarrow} c_{-k,\downarrow} c_{k,\uparrow} + c^{\dagger}_{-k,\downarrow} c^{\dagger}_{k,\uparrow} c_{k,\uparrow} c_{-k,\downarrow} + c^{\dagger}_{k,\uparrow} c_{k,\uparrow}. \end{aligned} \tag{1.6}$$

The act of inserting unity between terms allows one to readily see upon inspection that the first two terms in Eq. 1.6 are in fact equivalent by virtue of commutation of some of the operators present. It does not matter which particle we create or annihilate first, it only matters that we either create or annihilate first. That is to say we may interchange $c_{-k,\downarrow}$ with $c_{k,\uparrow}$, and similarly $c^{\dagger}_{-k,\downarrow}$ with $c^{\dagger}_{k,\uparrow}$ in the second term. Another argument revolves around the way Cooper pairs form. It is fact that $\hat{n}_{k,\uparrow}$ counts the occupation of electrons in the state $(k,\uparrow)$, while $\hat{n}_{-k,\downarrow}$ counts the occupation of the state $(-k,\downarrow)$. As Cooper pairs necessitate

the existence of an electron in state $(k,\uparrow)$ for each in state $(-k,\downarrow)$ and vice versa, it is clear that the last term in Eq. 1.6 can be dropped. Therefore with the use of Eq. 1.3 we find

$$\begin{aligned}\hat{n}_{k,\uparrow} + \hat{n}_{-k,\downarrow} &= 2n_{k,\uparrow} \\ &= 2c^{\dagger}_{k,\uparrow}c^{\dagger}_{-k,\downarrow}c_{-k,\downarrow}c_{k,\uparrow} \\ &= 2b^{\dagger}_{k}b_{k}. \end{aligned} \tag{1.7}$$

This expression allows us to absorb the spin degree of freedom from the reduced model Hamiltonian into the number operators. Doing so leaves us with a simplified expression:

$$H_{reduced} = \sum_{k} 2\epsilon_k b^{\dagger}_{k}b_{k} + \sum_{k}\sum_{k'} V_{k,k'}b^{\dagger}_{k'}b_{k}. \tag{1.8}$$

Now that we have simplified our model Hamiltonian it is of interest to evaluate commutation relation between $b^{\dagger}_{k}$ and b_k. We examine the quantity $[b_k, b^{\dagger}_{k'}]$.

$$[b_k, b^{\dagger}_{k'}] = [c_{-k,\downarrow}c_{k,\uparrow}, c^{\dagger}_{k',\uparrow}c^{\dagger}_{-k',\downarrow}]. \tag{1.9}$$

We can use fermion anti-commutation relations to simplify Eq. 1.9 into the following:

$$[b_k, b^{\dagger}_{k'}] = \delta_{k,k'}(1 - c^{\dagger}_{-k,\downarrow}c_{-k',\downarrow} + c^{\dagger}_{k',\uparrow}c_{k,\uparrow}) - 2c^{\dagger}_{k',\uparrow}\left\{c_{-k,\downarrow}, c^{\dagger}_{-k',\downarrow}\right\}c_{k,\uparrow}. \tag{1.10}$$

We now have two cases to interpret: first, when $k = k'$, and secondly, when $k \neq k'$. It can be shown that

$$[b_k, b^{\dagger}_{k'}] = \begin{cases} 0 & k \neq k' \\ 1 - (\hat{n}_{k,\uparrow} + \hat{n}_{-k,\downarrow}) & k = k'. \end{cases} \tag{1.11}$$

When $k \neq k'$, we would intuitively expect the commutation relation to be zero as this represents the case where the two particles being described do not form a Cooper pair. Derived in a similar fashion, it can be shown that the other commutation relations are:

$$[b_k, b_{k'}] = 0$$
$$[b_k^\dagger, b_{k'}^\dagger] = 0. \tag{1.12}$$

Londons' postulation of coherent states lead BCS to express the superconducting wavefunction as:

$$|\psi_0\rangle = \prod_k \frac{(1 + g_k b_k^\dagger)}{\sqrt{1 + |g_k|^2}} |0\rangle . \tag{1.13}$$

By applying the variation principle, we minimize the ground-state energy of the system. This is done through solving the following Lagrange multiplier problem:

$$\delta \langle\psi_0| H_{reduced} - \mu \sum_{k,\sigma} \hat{n}_{k,\sigma} |\psi_0\rangle = 0, \tag{1.14}$$

under the restriction that the average number of particles in the system be conserved, namely

$$\langle\psi_0| \sum_{k,\sigma} \hat{n}_{k,\sigma} |\psi_0\rangle = N. \tag{1.15}$$

The solution to this problem leads to particle (u_k) and hole (v_k) amplitudes given by

$$\begin{aligned} u_k^2 &= \frac{1}{2}(1 + \frac{\epsilon_k - \mu}{E_k}) \\ v_k^2 &= \frac{1}{2}(1 - \frac{\epsilon_k - \mu}{E_k}) \\ u_k v_k &= \frac{\Delta_k}{2E_k} \\ |u_k|^2 + |v_k|^2 &= 1 \\ E_k &= \sqrt{(\epsilon_k - \mu)^2 + \Delta_k^2}. \end{aligned} \tag{1.16}$$

The Lagrange multiplier, μ, is the chemical potential, E_k is the energy of the quasiparticle excitation, and Δ_k is the order parameter. The order parameter dictates an energy gap to be

overcome to create a quasiparticle in the superconducting state. It is self-consistently solved using

$$\Delta_k = -\sum_{k'} V_{k',k} \frac{\Delta_{k'}}{2E_{k'}}. \tag{1.17}$$

Additionally, it may also be shown that the BCS superconducting coherence length is given by

$$\xi_{BCS} = \frac{2\hbar v_f}{\pi \Delta}. \tag{1.18}$$

Despite the BCS theory being an incredibly successful and sufficient theory in many applications, it falls short in the fact that it is incapable of handling any sort of inhomogeneity which causes spatial variations in the order parameter due to its formulation in momentum space. The Ginzburg-Landau theory, though macroscopic and phenomenological, can describe inhomogeneous superconductivity. Although this theory would suffice in general, it is of no practical use in the research being conducted as it is only valid near the critical field and temperature. This limitation is far too restricting for topological superconductors as it is imperative that we have high stability of states. This may only be granted by near zero temperature and thus may only be adequately described through microscopic theories. Therefore it is essential that we use the BdG theory for our research. The BdG theory of superconductivity will be described in depth within Chapter 2.

1.4 Topological Superconductivity

Topological superconductors are a classification of materials that are capable of hosting Majorana fermions as zero-energy elementary excitations. In 1937 Ettore Majorana showed that there exists a manipulation of the Dirac equation wherein the resulting particles are in fact their own anti-particles [26]. Majorana fermions are non-Abelian quasiparticles and as such, do not obey traditional fermion or boson exchange statistics, but rather a set of quantum mechanical relations which are far more fundamentally complex and intriguing. Majorana

fermions live within unique systems; ones which possess two fascinating and ultimately useful properties which may be harnessed for technological advancement. The first being that these systems contain a large set of degenerate ground states which exhibit very little interaction with the surrounding environment. The second of which is where these particles inherit their name: for their non-commutative properties. While the wavefunction describing fermions or bosons undergoes a simple phase rotation under particle interchange, the wavefunctions describing non-Abelian quasiparticles undergoes a transformation from one ground state into another. Hence, multiple particle interchange operations continue to transform the wavefunction between ground states; the order in which they are applied being important.

The study of non-Abelian statistics is relatively new within the scientific community. In 1997, Russian physicist Alexei Kitaev showed that non-Abelian quasiparticles could theoretically be used to construct topological quantum computers [10] thus further kindling the world-wide interest in these curious systems. Kitaev did so by showing that the inherent characteristics which define non-Abelian quasiparticles are essentially analogous to those needed for topological quantum computation. Kitaevs work melds well with findings by Moore, Read [12], and Wen [4] as they have shown non-Abelian states can exist in the fractional quantum hall effect. The fractional quantum hall effect is not the only place in which these systems are theorized to manifest. P-wave superconductors [15] as well as topological insulators [9], and their combination called topological superconductors are also strong candidates.

In order to discuss and understand the properties of non-Abelian systems it is necessary to construct a context in which they are manifested and reasoning for their importance. Consider a two or three dimensional material with a select number of vortices passing through it; analogous to the vortex state of p-wave superconductors. Non-Abelian systems are capable of hosting the unique collection of the following properties:

1. The ground state of the system must be highly degenerate with respect to the number of vortices present.

2. The act of permuting vortices must cause the system to be transformed from one ground state into another.

3. There must exist a sizeable energy gap which serves to separate the ground state energy

from the rest of the energy spectrum present within the system.

4. Perturbations and noise must leave the degeneracy factor grossly unchanged and the energy gap must not collapse.

Todays society is highly motivated by technology and the speed in which it can provide answers. Silicon transistor technology has advanced significantly since its invention in 1947 at AT&T's Bell Laboratories, but is now being driven ever closer to its limits. Although current standards are quite impressive with a twenty-two nanometer channel length, there is little room left for further improvement due to quantum mechanical effects being exponentially dominant at these small lengths. Further shrinking the channel length vastly increases the quantum tunneling between contacts leading to a higher rate of faulty computation. Any computational method with a finite fault probability must be met with error correction, an expensive set of operations which defeat the purpose of improving the base computational rates, thus the reason why silicon technology is near its limits.

The thought and pursuit of some 'higher form' of computation is not new. Silicon's limitations have long been known and scientists have been working diligently to theorize and construct the next level – quantum computing. As of now, quantum computing exists only as an incomplete theoretical construct[2]. Topologically protected quantum computing holds the most promise to catapult society into a new era of computing. A two-dimensional system containing n non-Abelian anyons hosts an exponentially large topologically protected Hilbert space [17]. This topological protection leads to potential unfathomably low error rate which would warrant no need for quantum error correction algorithms.

The motivation behind quantum computing is clear: current technology is already being pushed to its limits, the computation time enhancement is unparalleled, and the sheer amount of data representation is staggering. In classical systems a bit represents one of two states, $|0\rangle$ or $|1\rangle$, whereas a quantum bit, a qubit, may host any superposition of the two states. This is to say a system of n bits may hold one of 2^n states while a system of n qubits holds any superposition of 2^n states. Thus, n qubits is computationally equivalent to 2^n bits which

[2]The company D-wave Systems currently has a working 512-qubit processor [7], although there remains some controversy as to whether or not it operates off truly quantum mechanical principles as current theory exists.

allows for truly unimaginably large scale computations to take place. The mathematics and process of using qubits for quantum computations is an intriguing field of study known as braid theory. The scope of this thesis precludes discussion of braid theory.

1.5 Majorana Equation

The purpose of this section is to introduce some of the theoretical foundations upon which the concept of non-Abelian quasiparticles stand on. Although non-Abelian quasiparticles have not been confirmed to exist it is theorized they may exist within fractional quantum Hall systems, p-wave superconductors, as well as hybrid systems. This section is dedicated to provide evidence for their existence and offer insight into how they may be observed and later used for topological quantum computing.

In 1991, Moore and Read [12] found the so-called Moore-Read Pfaffian wavefunctions from making use of conformal field theory to find trial wavefunction to the $\upsilon = \frac{5}{2}$ quantum Hall state. These wavefunctions are defined as follows [15]:

$$\psi_{Pf} = Pf\left(\frac{1}{z_i - z_j}\right)\prod_{i<j}(z_i - z_j)^m e^{-\sum_i \frac{|z_i|^2}{4\ell_0^2}}, \tag{1.19}$$

while the Pfaffian is found through

$$Pf\left(\frac{1}{z_i - z_j}\right) = A\left(\frac{1}{z_1 - z_2}\frac{1}{z_3 - z_4}...\right). \tag{1.20}$$

When the exponent m is even the wavefunction represents an even-denominator quantum Hall state occupying the lowest Landau level. These wavefunctions also represent an analogous p-wave superconducting system, thus it is sufficient to discuss them within the same context. The duo argue the quasiparticle excitations arising from this mathematical description are non-Abelian in nature. Numerical works done by Rezayi and Haldane [18] show that the first excited state of the $\upsilon = \frac{1}{2}$ fractional quantum Hall state represent the same universality class as the Moore-Read Pfaffian wave function thus lending merit to the claim that quasiparticle excitations obey non-Abelian exchange statistics. Rezayi and Haldane's results, among others [13], provide sufficient justification to state that if the $\upsilon = \frac{5}{2}$ state has the same universality

class as the Moore-Read Pfaffian state, then the $\upsilon = \frac{5}{2}$ states quasiparticle excitations are non-Abelian anyons.

Vortices in p-wave superconducting materials are thought to host Majorana operators [20], analogous to creation and annihilation operators for fermion or boson systems but for non-Abelian systems. Vortices can trap spin $\frac{1}{2}$ excitations which are known as Majorana zero modes. These Majorana zero modes hold an equal number of electrons and holes, therefore, the Majorana operators take the form $\gamma_i = c_i + c_i^\dagger$. As a result of the operator taking this form it is clear that Majorana fermions are in fact their own anti-particle. This can be shown through the Majorana equation, a modified Dirac equation. Dirac's equation is as follows:

$$\left(i\gamma^\mu \partial_\mu - m\right)\psi = 0 \tag{1.21}$$

with the convention that $\hbar = 1$ and $c = 1$. The γ^μ matrices are required to satisfy Clifford algebra, just as they do for the Dirac equation. This means that the following equations must hold [26] [20]:

$$\{\gamma^\mu \gamma^\nu\} = 2\eta^{\mu\nu} \tag{1.22}$$

$$\begin{aligned}
\left(\gamma^0\right)^2 &= 1 \\
-\left(\gamma^1\right)^2 &= 1 \\
-\left(\gamma^2\right)^2 &= 1 \\
-\left(\gamma^3\right)^2 &= 1.
\end{aligned} \tag{1.23}$$

Majorana found a set of γ matrices which are purely imaginary for spin $\frac{1}{2}$ particles, thus leading to a particle which is its own anti-particle. The matrices are [25]:

$$\begin{aligned}
\tilde{\gamma}^0 &= \sigma_2 \otimes \sigma_1 \\
\tilde{\gamma}^1 &= i\sigma_1 \otimes 1 \\
\tilde{\gamma}^2 &= i\sigma_3 \otimes 1 \\
\tilde{\gamma}^3 &= i\sigma_2 \otimes \sigma_2,
\end{aligned} \tag{1.24}$$

with $\sigma_i's$ being the Pauli spin matricies. Thus, Majorana's equation is simply:

$$(i\tilde{\gamma}^{\mu}\partial_{\mu} - m)\,\tilde{\psi} = 0. \tag{1.25}$$

The fact that $\gamma_i^2 = 1$ indicates that purely real solutions obey non-Abelian statistics. Majorana modes may be superimposed upon one another in order to create fermionic operators through the relation $f_i = \frac{\gamma_1 + i\gamma_2}{2}$, with occupation number $n_i = f_i f_i^{\dagger}$. Therefore, a system hosting $2N$ Majorana zero modes has an equivalent N fermionic operators whose degenerate ground states can be written as $|n_0, n_1, n_3, ..., n_N\rangle$. If an action is then applied to the system such that Majorana modes are interchanged, corresponding to parts of fermionic operators being swapped, then in general the system will no longer be in the same ground state. Thus, as braiding vortices interchanges Majorana zero modes, the system transforms between ground states. It is theorized Majorana zero modes may exist in systems exhibiting spin-orbit coupling in two dimensional conductors [21]. When this two dimensional conductor is placed within close proximity to a three dimensional superconducting body, there will be a superconducting effect induced within the conductor. This phenomena is called the proximity effect.

1.6 Outline

The remaining chapters of this thesis are arranged as follows. Chapter 2 discusses the necessary theoretical background for studying superconductivity and vortex states in addition to numerical techniques. Chapter 3 focuses on the study of a new class of materials known as topological superconductors. Here we will present our model for studying these materials and the necessary framework for understanding the new parameters which will be introduced. This chapter concludes in reproducing results calculated from a Green's function approach using our self-consistent BdG formulation. The most significant results are presented in Chapter 4. Here we discuss the differences between Abelian and non-Abelian topological phases in the context of the coexistence of topological superconductivity and vortex states. Finally, Chapter 5 will conclude this thesis.

Chapter 2

Formulation

The purpose of this chapter is to acquaint the reader with the necessary theoretical framework for the research. This chapter includes a preliminary derivation of the real-space generalization of the BCS theory of superconductivity known as the BdG theory of superconductivity. Followed by a discussion of the theory for TSC. The chapter concludes with an overview of the advanced numerical techniques that are used to expedite computations.

2.1 Bogoliubov de-Gennes Theory of Superconductivity

In the presence of an inhomogeneity, momentum is no longer conserved. Because of this technicality we must formulate our theory in real space. The BdG theory under a tight-binding framework provides everything we desire: a low temperature real space formulation that is a generalization of BCS theory. It benefits from numerically efficient implementation in addition to providing a means to control chemical potential.

The model Hamiltonian is given by:

$$H = \sum_{<i,j>\sigma} t_{i,j} c^{\dagger}_{i,\sigma} c_{j,\sigma} + \sum_{i,\sigma} (\epsilon_i - \mu) \hat{n}_{i,\sigma} + \sum_{i} U_{i,i} \hat{n}_{i,\uparrow} \hat{n}_{i,\downarrow} + \frac{1}{2} \sum_{<i,j>} \sum_{\sigma,\sigma'} U_{i,j} \hat{n}_{i,\sigma} \hat{n}_{j,\sigma'}. \qquad (2.1)$$

This model allows electrons at site j to 'hop' to site i with an amplitude of $t_{i,j}$. This is done through the creation and annihilation of electrons with spin σ. Electron filling is controlled by the chemical potential μ. Impurities are represented by non-zero elements of ϵ_i. $U_{i,i}$ is the on-site s-wave electron interaction potential, while $U_{i,j}$ is the off-site d-wave potential. Interfaces

are taken into consideration through a combination of modifications to $t_{i,j}$, $U_{i,i}$ and $U_{i,j}$. In general the Hamiltonian given in Eq. 2.1 is impossible to solve exactly. Due to this fact it is essential that we approximate the interaction terms through the use of mean-field theory, which then needs to be iteratively converged. The two-body number operator interactions are replaced with its average value plus a first order approximation to the fluctuation around that average. Mathematically speaking:

$$\hat{n}_{i,\sigma}\hat{n}_{i,\sigma'} = \left\langle \hat{c}^{\dagger}_{i,\sigma}\hat{c}_{i,\sigma}\hat{c}^{\dagger}_{i,\sigma'}\hat{c}_{i,\sigma'} \right\rangle + \left(\hat{c}^{\dagger}_{i,\sigma}\hat{c}_{i,\sigma}\hat{c}^{\dagger}_{i,\sigma'}\hat{c}_{i,\sigma'} - \left\langle \hat{c}^{\dagger}_{i,\sigma}\hat{c}_{i,\sigma}\hat{c}^{\dagger}_{i,\sigma'}\hat{c}_{i,\sigma'} \right\rangle \right). \tag{2.2}$$

With the use of Wick's theorem,

$$\begin{aligned} \left\langle \hat{c}^{\dagger}_{i,\sigma}\hat{c}^{\dagger}_{i,\sigma'}\hat{c}_{i,\sigma'}\hat{c}_{i,\sigma} \right\rangle = & \left\langle \hat{c}^{\dagger}_{i,\sigma}\hat{c}_{i,\sigma} \right\rangle \left\langle \hat{c}^{\dagger}_{i,\sigma'}\hat{c}_{i,\sigma'} \right\rangle \\ & - \left\langle \hat{c}^{\dagger}_{i,\sigma}\hat{c}_{i,\sigma'} \right\rangle \left\langle \hat{c}^{\dagger}_{i,\sigma'}\hat{c}_{i,\sigma} \right\rangle \\ & + \left\langle \hat{c}^{\dagger}_{i,\sigma}\hat{c}^{\dagger}_{i,\sigma'} \right\rangle \left\langle \hat{c}_{i,\sigma'}\hat{c}_{i,\sigma} \right\rangle, \end{aligned} \tag{2.3}$$

we may rewrite the model Hamiltonian to an effective Hamiltonian after a significant amount of manipulation as

$$\begin{aligned} H_{effective} = & \sum_{<i,j>\sigma} t_{i,j}c^{\dagger}_{i,\sigma}c_{j,\sigma} + \sum_{i,\sigma}(\epsilon_i - \mu)\hat{n}_{i,\sigma} \\ & + \sum_{i,\sigma} V^{H}_{i,i}\hat{n}_{i,\sigma} + \frac{1}{2}\sum_{<i,j>\sigma} V^{H}_{i,j}\hat{n}_{i,\sigma} \\ & - \frac{1}{2}\sum_{<i,j>\sigma} V^{F}_{i,j}\hat{c}^{\dagger}_{i,\sigma}\hat{c}_{j,\sigma} + \sum_{i} \Delta_{i,i}\hat{c}^{\dagger}_{i,\uparrow}\hat{c}^{\dagger}_{i,\downarrow} \\ & + \frac{1}{2}\sum_{<i,j>} \Delta_{i,j}\hat{c}^{\dagger}_{i,\uparrow}\hat{c}^{\dagger}_{j,\downarrow} + H.c.. \end{aligned} \tag{2.4}$$

Where the Hartree potential, V^H, comes from the electron density distribution throughout the lattice. The Fock potential, V^F, describes particle exchange effects. Its purpose is to force antisymmetric wavefunctions by lowering binding energy to ensure adherence to the Pauli exclusion principle. The s and d-wave order parameters are represented by $\Delta_{i,i}$ and

$\Delta_{i,j}$ respectively. These parameters are the mean-fields that fallout from the derivation of this Hamiltonian. They are defined by the following:

$$V_{i,i}^{H} = U_{i,i} \left\langle \hat{c}_{i,\sigma}^{\dagger} \hat{c}_{i,\sigma} \right\rangle \tag{2.5}$$

$$V_{i,j}^{H} = U_{i,j} \left\langle \hat{c}_{j,\sigma}^{\dagger} \hat{c}_{j,\sigma} \right\rangle \tag{2.6}$$

$$V_{i,j}^{F} = \frac{1}{2} U_{i,j} \left[\left\langle \hat{c}_{j,\sigma}^{\dagger} \hat{c}_{i,\sigma} \right\rangle + \left\langle \hat{c}_{i,\sigma}^{\dagger} \hat{c}_{j,\sigma} \right\rangle \right] \tag{2.7}$$

$$\Delta_{i,i} = U_{i,i} \left\langle \hat{c}_{i,\downarrow} \hat{c}_{i,\uparrow} \right\rangle \tag{2.8}$$

$$\Delta_{i,j} = \frac{1}{2} U_{i,j} \left[\left\langle \hat{c}_{j,\downarrow} \hat{c}_{i,\uparrow} \right\rangle + \left\langle \hat{c}_{i,\downarrow} \hat{c}_{j,\uparrow} \right\rangle \right]. \tag{2.9}$$

We can rewrite Eq. 2.4 into a matrix equation which is more commonly known as the BdG equations.

$$\begin{pmatrix} \hat{T} + \hat{V}^{(H)} + \hat{V}^{(F)} & \hat{\Delta} \\ \hat{\Delta}^{\star} & -\left(\hat{T}^{\star} + \hat{V}^{(H)} + \hat{V}^{(F)} \right) \end{pmatrix} \begin{pmatrix} u_n \\ \\ v_n \end{pmatrix} = \epsilon_n \begin{pmatrix} u_n \\ \\ v_n \end{pmatrix} \tag{2.10}$$

The heart of our research revolves around solving these equations to self-consistently converge the mean-fields eqs. (2.5) to (2.9). We make use of highly efficient parallelizable routines to expedite computation. These methods are discussed in detail later in this thesis.

2.2 Vortex Lattice

When an electron moves in a magnetic field, $\mathbf{B}(\mathbf{r}, t) = \nabla \times \mathbf{A}(\mathbf{r}, t)$, the quantum mechanical momentum is subsequently changed from $\frac{\mathbf{p}}{m}$ to $\frac{\mathbf{p} + \frac{e}{c}\mathbf{A}(\mathbf{r},t)}{m}$. The extra term in the momentum equation in an additional multiplicative factor in the particles' wavefunction. According to the path-integral formulation of quantum mechanics,

$$\begin{aligned} \psi(\mathbf{r}, t) &= \int d\mathbf{r}' dt' K(\mathbf{r}, t; \mathbf{r}', t') \psi(\mathbf{r}', t') \\ K(\mathbf{r}, t; \mathbf{r}', t') &\propto \sum_{all\ \ paths(\mathbf{r}', t') \to (\mathbf{r}, t)} e^{\frac{i}{\hbar} S(\mathbf{r}, t; \mathbf{r}', t')}, \end{aligned} \tag{2.11}$$

where $S(\mathbf{r}, t; \mathbf{r}', t')$ is the classical action of the particle. In the presence of a vector potential, $\mathbf{A}(\mathbf{r}, t)$, the wavefunction picks up the term

$$\exp\left(i\frac{-e}{\hbar c}\int_{path} d\mathbf{l}\cdot\mathbf{A}(\mathbf{r}, t)\right). \tag{2.12}$$

And hence, the hopping amplitudes are altered [22];

$$t_{i,j} \to \tilde{t_{i,j}} = t_{i,j}\exp\left(i\frac{\pi}{\phi_0}\int_{\mathbf{r}_i}^{\mathbf{r}_j} d\mathbf{r}\cdot\mathbf{A}(\mathbf{r}, t)\right), \tag{2.13}$$

where the quantity ϕ_0 represents the flux quantum in the superconducting state and is given by $\phi_0 = \frac{hc}{2e}$. This additional factor is often referred to as the Peierls factor [22] [23]. Consider a square superconducting body subject to a magnetic field $\mathbf{H} = H\hat{z}$ under the symmetric gauge, $\mathbf{A}(\mathbf{r}) = \frac{1}{2}\mathbf{H}\times\mathbf{r}$. Consider the lattice to have a total of m_ϕ flux quantua passing through it; hence $HL_xL_ya^2 = m_\phi\phi_0$. The resulting adjustments must be made to the hopping elements

$$\begin{aligned}\tilde{t_{i,j}} &= t_{i,j}\exp\left(i\frac{\pi m_\phi}{2L_xL_y}\int_{\mathbf{r}_i}^{\mathbf{r}_j}(dx, dy, 0)\cdot(-y, x, 0)\right)\\ &= t_{i,j}\exp\left(i\frac{\pi m_\phi}{2L_xL_y}\left(-y_i(x_j - x_i) + x_i(y_j - y_i)\right)\right).\end{aligned} \tag{2.14}$$

We then define a Bravais lattice vector $\mathbf{R} = m\hat{u}_1 + n\hat{u}_2 = (mL_y, nL_x)$ of the vortex lattice, where m and n are integers. We also define the vortex core to be located at $\mathbf{r}_{centre} = \mathbf{r}_0 + \frac{1}{2}(L_x, L_y)$ where $\mathbf{r}_0$ is an offset vector. Under periodic boundary conditions for the vortex lattice, we find

$$\begin{aligned}u(\mathbf{r} + \mathbf{R}) &= u(\mathbf{r})\exp\left(i\frac{\chi(\mathbf{r}, \mathbf{R})}{2}\right),\\ v(\mathbf{r} + \mathbf{R}) &= v(\mathbf{r})\exp\left(-i\frac{\chi(\mathbf{r}, \mathbf{R})}{2}\right),\end{aligned} \tag{2.15}$$

where $\chi(\mathbf{r}, \mathbf{R})$ is given by [23]

$$\chi(\mathbf{r}, \mathbf{R}) = -\frac{2\pi}{\phi_0}\mathbf{A}(\mathbf{R})\cdot\mathbf{r} - \pi mn + \frac{2\pi}{\phi_0}(\mathbf{H}\times\mathbf{r}_0)\cdot\mathbf{R}. \tag{2.16}$$

As a result of this formulation, all hopping elements are modified according to Eq. 2.14, from site i to site j, with periodic entries of the Hamiltonian (Eq. 2.10) being further modified using Eq. 2.15.

2.3 Numerical Techniques

Our research is focused on computing self-consistent solutions of eigenvalue problems created by examining a variety of superconducting systems. As such, we are forced to diagonalize Eq. 2.10 as many times as necessary to obtain fully converged results. This desire is quite costly as the computational complexity of the generalized eigenvalue problem is $\mathcal{O}(n^3)$, a price which is too costly to examine any system of significant size. As a result several advanced numerical techniques are employed in order to improve the efficiency of our calculations and hence the effectiveness of our research. We make use of a kernel polynomial expansion scheme to self-consistently solve the mean-fields Eqs. 2.5, 2.6, 2.7, 2.8, and 2.9 reducing the computational complexity to $\mathcal{O}(n^2)$. This is followed by application of the Sakurai-Sugiura (SS) matrix size reduction method to extract eigenvalues within a specified range.

2.3.1 The Chebyshev Kernel Polynomial Expansion Scheme

Solving the BdG equation (Eq. 2.10) is typically done by directly diagonalizing the BdG Hamiltonian to obtain the full eigenpair spectrum. This spectrum would then be used to self-consistently evaluate the mean-fields. However, due to our interests in Majorana fermions we require only the part of the spectrum that is in a small window around zero energy. This small technicality frees us of the computational burden of direct diagonalization and allows us to explore polynomial expansion schemes. The Chebyshev polynomials are defined by the following relations:

$$\begin{aligned} q_1 &= \hat{K} q_0 \\ q_n &= 2\hat{K} q_{n-1} - q_{n-2}, \end{aligned} \tag{2.17}$$

where the seeding vector (q_n) is given by $e_0 = \begin{pmatrix} I \\ 0 \end{pmatrix}$ and $h_0 = \begin{pmatrix} 0 \\ I \end{pmatrix}$ for computing $\left\langle c_i^\dagger c_j \right\rangle$ and $\langle c_i c_j \rangle$ respectively. $\hat{K}$ is the scaled Hamiltonian given by $\hat{K} = \frac{\hat{H} - bI}{a}$. Where a and b are material dependent parameters calculated by $a = \frac{E_{max} + E_{min}}{2}$ and $b = \frac{E_{max} - E_{min}}{2}$, although it is generally sufficient to estimate these parameters. We keep a total of n terms in the expansion. Expanding the Hamiltonian with this set of orthonormal polynomials allows us to define the mean-fields through the following relations:

$$\begin{aligned} \langle c_i c_j \rangle &= \sum_n \tau_n h_{i,j,n} \\ \left\langle c_i^\dagger c_j \right\rangle &= \sum_n \tau_n e_{i,j,n}, \end{aligned} \tag{2.18}$$

where τ_n are the inner product weighting factors which are given by the following relations at zero temperature:

$$\tau_n = \begin{cases} \frac{\pi - cos^{-1}(-\frac{b}{a})}{\pi} & \text{if } n = 0 \\ \frac{-sin(ncos^{-1}(-\frac{b}{a})}{\frac{n\pi}{2}} & \text{if } n \neq 0 \end{cases}, \tag{2.19}$$

or at finite temperatures by the equation:

$$\tau_n = \int dx \frac{1}{1 + e^{\frac{ax+b}{T}}} \frac{1}{\sqrt{1 - x^2}} \cos\left(n \cos^{-1}(-x)\right) w. \tag{2.20}$$

The inner product weighting factor may optionally be scaled by a kernel to change the rate and smoothness of convergence. The kernels are as follows:

$$\tau_n = \begin{cases} \tau_n & Dirichlet \\ \tau_n \frac{sinh(\lambda(1 - \frac{n}{n_c - 1}))}{sinh(\lambda)} & Lorentz \\ \tau_n (1 - \frac{n}{n_c - 1}) & Fejer \\ \tau_n sin^M(\frac{\pi n}{n_c - 1}) & Lanczos \end{cases}. \tag{2.21}$$

We iteratively perform self-consistent calculations until suitable convergence criterion has been reached. We consider the system to be converged when $\frac{\sum|<c_ic_j>_{new}-<c_ic_j>_{old}|}{\sum|<c_ic_j>_{old}|} \leq \epsilon$ and $\frac{\sum|<c_i^\dagger c_j>_{new}-<c_i^\dagger c_j>_{old}|}{\sum|<c_i^\dagger c_j>_{old}|} \leq \epsilon$ for some suitably small ϵ.

To ensure this method provides reasonable results we must compare to the traditional DD method. Our first test is to tweak the guessed parameters of a, b, and to fine tune the number of terms, n_c. This is done by varying our parameters until a result is found that closely approximates the exact direct diagonalization (DD) result. We first examined a 24×24 periodic lattice under the s-wave superconducting regime. Testing[1] leads us to use $n_c = 800$ terms, $a = 12$, $b = 0$, and the Dirichlet kernel as the input parameters to the Chebyshev kernel polynomial expansion (CKPE) method. One may see from Fig. 2.1 that these specifications provide the closest approximation to DD.

One might equally well make use of the Legendre polynomials,

$$P_{n+1}(x) = \frac{2n+1}{n+1}xP_n(x) - \frac{n}{n+1}P_{n-1}(x). \tag{2.22}$$

Though these polynomials provide an immediate, and a more subtle hindrance as compared to the Chebyshev polynomials. The expansion terms appearing in Eq. 2.17 are 2, and -1 respectively, whereas they are $\frac{2n+1}{n+1}$ and $\frac{n}{n+1}$ in Eq. 2.22. As far as computer architecture is concerned, multiplying by 2 corresponds to a simple bit shift, whereas multiplying by -1 corresponds to taking the twos compliment. Both these procedures are significantly less computationally intensive than the corresponding Legendre polynomial requirements. The more subtle difference is the fact that Chebyshev polynomials are generally believed to give the best resistance to Runge's phenomenon [16]. Hence, the Chebyshev polynomials are used in an effort to reduce Runge's phenomenon in addition to providing a computationally more efficient algorithm.

[1]For a more in-depth analysis of choosing n_c, a, and b see Appendix A

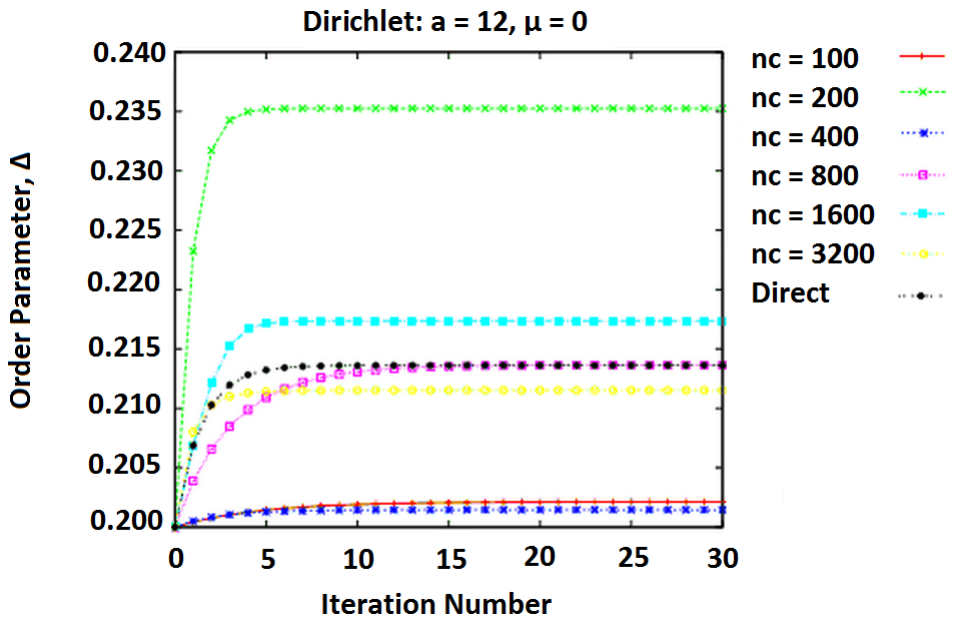

Figure 2.1: Magnitude of the Order Parameter varying the number of terms in the Chebyshev expansion.

We are forced to calculate the LDOS at this point due to the loss of information incurred as a result of invoking the SS method. Due to our interests in low-energy states we may use it as a means of probing lattice sites to determine localization of these states. Energy states by their inherent nature have a precise value which is represented by an infinitesimally small width on a LDOS plot. As a consequence of this fact we must incorporate a smoothing width in our calculations to ensure we retain information from all energy states within the window of interest. We make use of a LDOS calculation technique by Covaci et al. [6]:

$$LDOS_i(x) = \sum_{n=0}^{n_c} \frac{1}{a} \frac{1}{\sqrt{1-x^2}} \frac{2-\delta_{n,0}}{\pi} \cos(n \cos^{-1}(x)) e_{n,i} \frac{\sinh(\upsilon(1-\frac{n}{n_c}))}{\sinh(\upsilon)}, \tag{2.23}$$

where i is the site for which we are calculating the LDOS, a is the same parameter used during the rest of the CKPE method, and υ is the Lorentzian smoothing width. The parameter x is a renormalized energy. If we wish to calculate the LDOS between $\pm E$, then $-E \leq \frac{x}{a} \leq E$.

2.3.2 The Sakurai-Sugiura Matrix Size Reduction Method

The SS method is a way to extract a set range of eigenpairs from a matrix by means of applying a set of unitary transforms. Due to Majorana fermions existing as zero-energy bound states, the SS method is a perfect tool for us to use to examine a small window around zero energy. The SS method constructs a Krylov subspace in which we take an energy-space contour integral over a specific energy range. The result allows us to extract eigenpair information from the model Hamiltonian that is used to construct unitary transform matrices which are then used to reduce the size of the model Hamiltonian. The resulting Hamiltonian then contains only the information of the eigenpairs which lie inside of the specified contour.

We begin the SS method through defining L_0, M, N_q, γ , α, ρ, κ. These parameters determine the size of intermediate matrices and the shape, size, and location of the contour integral. We then set a sampling matrix of linearly independent columns as $\hat{V} = \{\nu^1, \nu^2, ..., \nu^{L_0}\}\epsilon\{-1, 1\}$. We then solve the age-old inverse problem through the use of either a conjugate gradient or multi-mass shifted conjugate gradient method. We need to solve

$$\left(z_j I - \hat{H}\right) \hat{Y}_j = \hat{V}, \tag{2.24}$$

where the contour is defined by

$$\begin{aligned} z_j &= \gamma + \rho(\cos(\theta_j) + i\alpha \sin(\theta_j)) \\ \omega_j &= \alpha \cos(\theta_j) + i \sin(\theta_j) \\ \theta_j &= \frac{2\pi}{N_q}\left(j - \frac{1}{2}\right). \end{aligned} \tag{2.25}$$

We then use the solution to the inverse problem to construct the moment matrix S_k. Any eigenpair that resides within the contour integral as defined by Eq. 2.25 will appear within the moment matrix as a non-zero quantity. Any eigenpair that does not reside within the contour integral contributes nothing to the moment matrix:

$$\hat{S}_k = \frac{1}{N_q}\sum_{j=1}^{N_q} \rho\omega_j z_j^k \hat{Y}_j. \tag{2.26}$$

We can then use the moment matrix to update our guess of the Krylov subspace size, L_0, through the following equations

$$\begin{aligned} \tilde{m_s} &= \frac{1}{L_0}\sum_{i=1}^{L_0} \left(\nu^i\right)^T s_0^i \\ L &= \lceil \frac{\kappa \tilde{m_s}}{M} \rceil. \end{aligned} \tag{2.27}$$

After updating L we redistribute sampling vectors as $\hat{V} = \{\nu^1, \nu^2, \ldots, \nu^L\}\epsilon\{-1, 1\}$ and proceed to compute the moment matrix again by reapplying Eqs. 2.24 and 2.26. We then take the ordered singular value decomposition of the moment matrix to obtain the right and left handed singular matrix along with the singular values according to Eq. 2.28,

$$\hat{U}\hat{\Sigma}\hat{V}^\dagger = SVD(\hat{S}), \tag{2.28}$$

$\hat{U}$ is the left-handed singular matrix, $\hat{V}$ is the right-handed singular matrix, and Σ's diagonal elements contain the singular values of $\hat{S}$. Σ's entries, σ_i, reflect the relative importance of the eigenpairs contianed within the contour integral. Each σ_i is strictly greater than or equal to zero and ordered such that $\sigma_i > \sigma_{i+1}$. We find m_s such that there exists m_s eigenpairs inside of the specified contour. If an eigenpair is inside of the contour its corresponding σ is strictly non-zero while eigenpairs residing outside of the contour boundary have a corresponding σ of exactly zero. Mathematically,

$$m_s : \frac{\sigma_j}{\sigma_1} \leq \delta : 1 \leq j \leq m_s. \tag{2.29}$$

The singular matrices are ordered such that the i^{th} column corresponds to σ_i. Thus, through taking the first m_s columns of the left-handed singular matrix we may reduce the size of the model Hamiltonian Eq. 2.4 according to the following equations:

$$\tilde{Q} = \hat{U}_{:,1:m_s}$$
$$\tilde{H} = \tilde{Q}^{\dagger}\hat{H}\tilde{Q}, \tag{2.30}$$

where $\tilde{H}$ is the reduced Hamiltonian. $\tilde{H}$ contains only the information of $\hat{H}$ that resides inside of the specified contour and exactly zero of the information that resides outside of that contour. The result is that $\tilde{H}$ is significantly smaller is size that $\hat{H}$ and therefore computationally less expensive to compute the eigenpairs.

2.3.3 Parallel Programming

Making use of the CKPE and SS methods is truly only viable in the case of $N = 2L_xL_y > n_c$, where L_x and L_y are the number of atomic lattice sites in the X and Y-direction respectively, and n_c is the number of terms kept within the CKPE method. However, due to subtle aspects within the formulation for both the CKPE and SS methods, we may incorporate massive parallelism within the heart of our computations. In particular, Eqs. 2.17, 2.24, and 2.26 are exposed to massive parallelism. There are several [2] additional instances where parallel programming methodologies may be incorporated; though the increased efficiency is significantly lower than the aforementioned cases.

There are two primary paradigms of parallel programming: shared, and distributed memory architectures. Modern personal computers are the prototypical example of shared memory architecture systems. An arbitrary number of processors may access the information stored within Random Access Memory (RAM). Distributed memory architectures may be thought of as two or more shared memory systems that are working in unison. Data that is stored in RAM on one machine is not necessarily stored in RAM of another machine. Hence any data required by a given processor must be sent to that processor from any number of others though specialized interfaces.

[2] Purely technically speaking the IPWF's, Eqs. 2.19, and 2.20 may also be programmed in a parallel structure though there is little benefit from doing so. The parallelism contained within Eq. 2.26 is an inherited aspect of Eq. 2.24. Equation 2.30 is also programmed in parallel though in a round-about fashion through the incorporation of multi-contours.

High level tools have been developed and are openly available for use to assist programmers in making the most of resources at hand. Open Multi-Processing (OMP) is used for shared memory systems while Message Passing Interface (MPI) is used for distributed memory systems.

2.3.4 Multiple Contours

The entirety of the SS method may be placed into an additional level of parallelism due to form of our Hamiltonian. The BdG matrix appearing in Eq. 2.10 is a Hermitian matrix, and as such contains purely real eigenvalues. This allows us to deconstruct Eq. 2.25 into a finer set of sub-contours provided that the union of sub-contours encompasses the same eigenvalues as the original contour. If we perform the following set of transformations,

$$\begin{aligned}
\alpha \to \alpha_{proc} &= \frac{\alpha\rho \sin\left(\cos^{-1}\left(\frac{\gamma_{proc}-\gamma}{\rho}\right)\right)}{\rho_{proc}} \\
\gamma \to \gamma_{proc} &= -\rho + \rho_{proc} + \gamma + \frac{2\rho}{N_{proc}} n \\
\rho \to \rho_{proc} &= \frac{\rho}{N_{proc}} \\
z_j \to z_{j,proc} &= \gamma_{proc} + \rho_{proc}(\cos(\theta_j) + i\alpha_{proc}\sin(\theta_j)) \\
\omega_j \to \omega_{j,proc} &= \alpha_{proc}\cos(\theta_j) + i\sin(\theta_j) \\
\theta_j &= \frac{2\pi}{N_q}\left(j - \frac{1}{2}\right),
\end{aligned} \tag{2.31}$$

we can construct a set of contours that satisfy our conditions, depicted in Fig. 2.2.

The implications of performing this transformation are subtle. Equations 2.28, 2.30, and the subsequent DD procedure are operations that either can not inherently be programmed in a parallel fashion, or the parallelization is not of great benefit. This method allows us to create many contours, each of which have their own unique singular value decomposition, m_s, $\tilde{Q}$, $\tilde{H}$, and eigenvalue decomposition procedures. Hence, we have created an artificial level of parallelism around the entirety of the SS method.

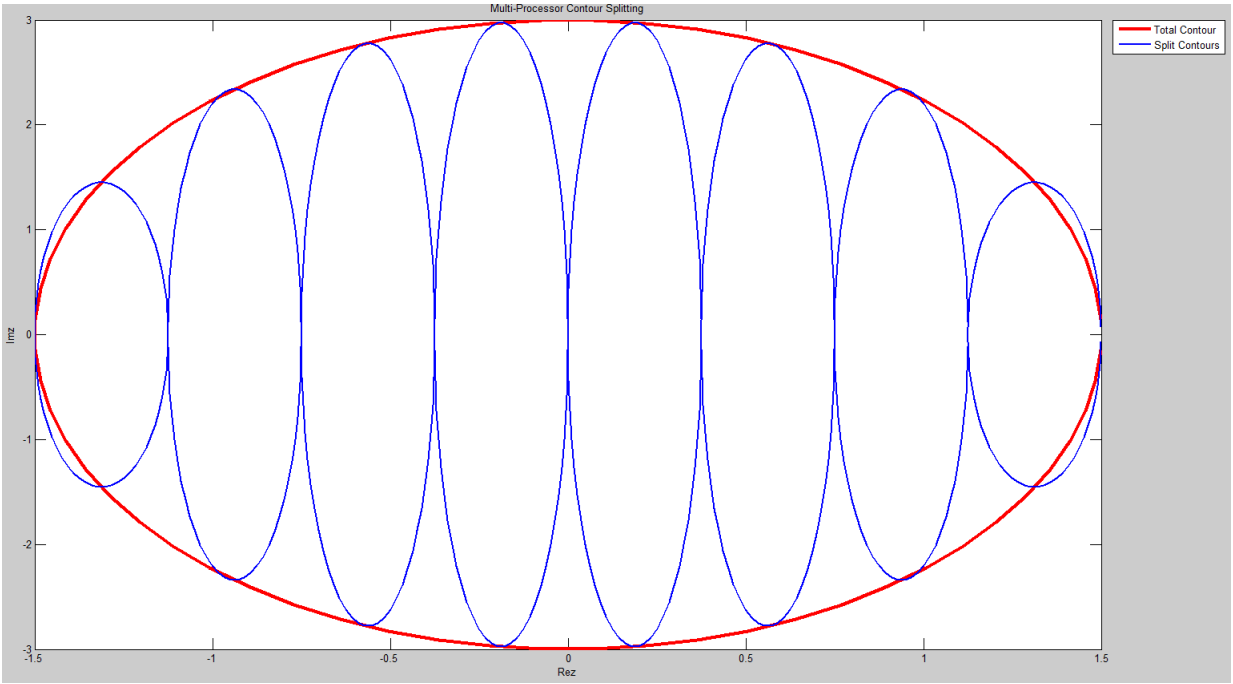

Figure 2.2: The user specified contour (red) split into eight sub-contours (blue) each covering a uniform eigenvalue range.

2.4 Verification of Methodologies

It is essential that we confirm the validity of our methodologies through recreation of traditional results. Our first task is to model a pure periodic s-wave superconducting body. This was done in Fig. 2.1, and is used as the calibration tool for our model. We have verified that our model closely approximates the standard model through appropriate choices of a, b, and n_c.

Our second verification procedure is to model a square lattice containing a single impurity located at the centre. We expect some distortion of the order parameter around the impurity with the extent of the distortion correlating to the magnitude of the impurity strength. We examine a 21×21 periodic s-wave lattice with a single impurity located at the centre. The on-site pairing potential is $V_{i,i} = -2.2t$, and the chemical potential is $\mu = 0$. For simplicity, we consider only nearest-neighbour interactions.

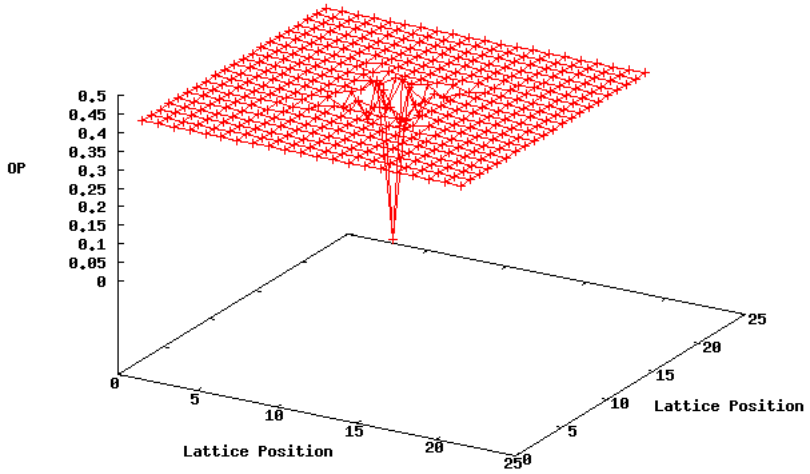

(a) $V_{imp} = 5.0t$

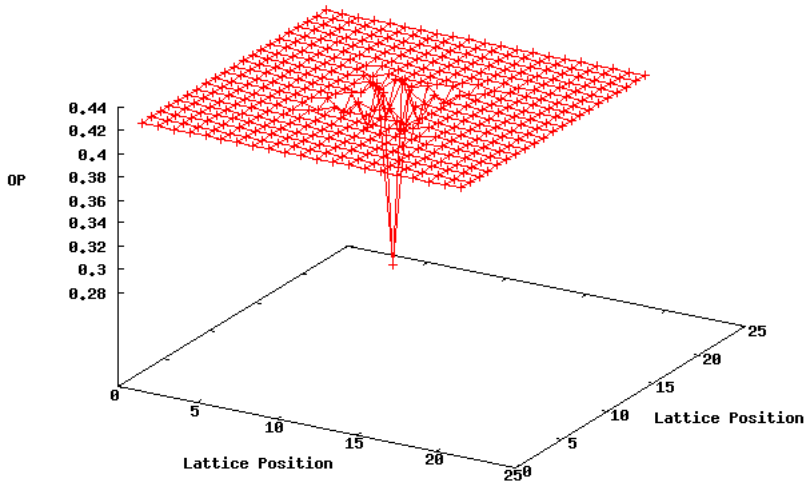

(b) $V_{imp} = 1.0t$

Figure 2.3: Order parameter structure for a single impurity lattice with impurity strength $V_{imp} = 5.0t$, and $V_{imp} = 1.0t$.

As we may see, the local order parameter for the $V_{imp} = 1.0t$ is distorted significantly less than when $V_{imp} = 5.0t$ around the impurity site. The lattice sites diagonally away from the

impurity site are effected more than those along either the $\hat{e_x}$ or $\hat{e_y}$ directions.

Finally, we wish to show that our model can accurately depict the finer structure of superconducting properties that arise from the proximity effect. This effect may be studied through examination of a superconducting - non-superconducting - superconducting (SNS) junction. This type of junction may be thought of as a thin layer of a non-superconducting material that has been placed between to identical superconducting materials.

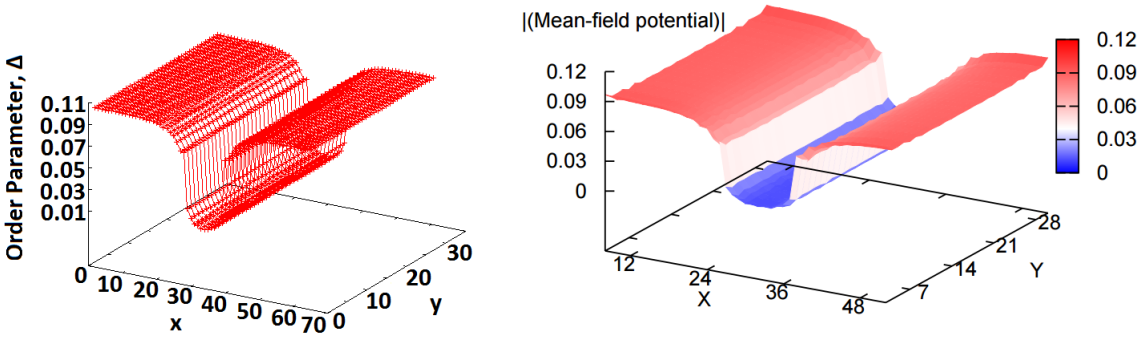

(a) Full SNS Junction.

(b) Full SNS Juntion. Data from the works of Nagai *et al.* [27].

Figure 2.4: Figure 2.4a generated from a 64×32 periodic s-wave lattice with on-site pairing potential $V_{i,j} = -2.2t\delta_{i,j}$, chemical potential $\mu = -1.5t$ at zero temperature. The normal conducting region is defined as $\{x \mid x \in 27 \leq x \leq 37 \forall y\}$. The hopping between superconducting regions is t, while hopping between superconducting and non-superconducting regions is $t' = 0.8t$.

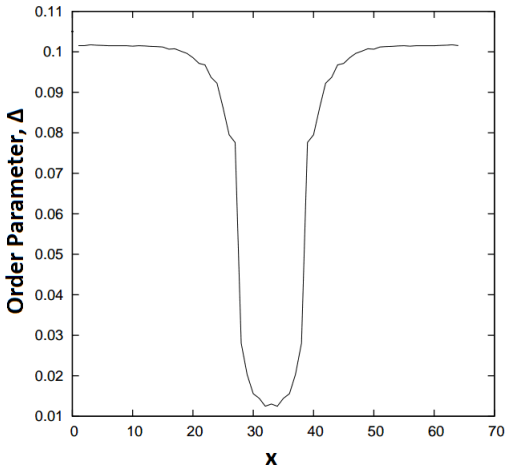

(a) SNS Junction slice at $y = 16$.

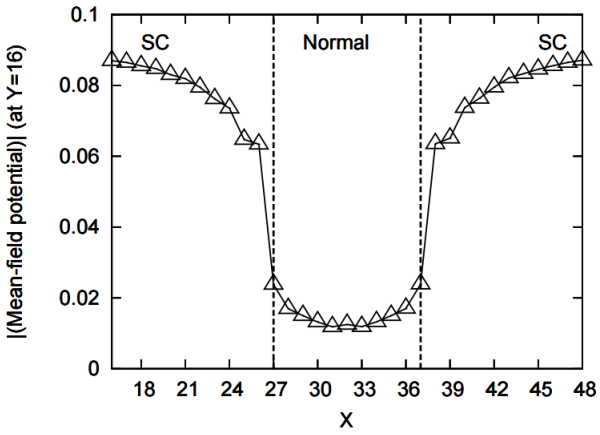

(b) SNS Junction slice at $x = 16$. Data from the works of Nagai *et al.* [27].

Figure 2.5: Cross sectional view of Figs. 2.4a and 2.4b at $y = 16$.

Figures 2.4a and 2.4b depict the absolute value of the mean-field potential as a function of atomic site. Although our results are slightly larger in magnitude than those of our mentors; significant conclusions may be drawn from them. The differences may arise from a number of sources: the Chebyshev parameters a, b, and n_c, the total number of self-consistent iterations allowed, the convergence criterion, etc .... We assume these differences may be ignored for the purposes of our discussion. We note the order parameter approaches, but does not reach zero in the normal region. This indicates that the two slabs of superconducting material have induced a superconducting effect within the normal material. Figures 2.5a and 2.5b depict a cross sectional view at $y = 16$.

Chapter 3

Topological Superconductivity

The purpose of this chapter is to familiarize the reader with the necessary theoretical framework of topological superconductivity (TSC). This chapter includes a brief description of the model Hamiltonian in both real and momentum space, followed by preliminary non-self-consistent results using the CKPE and SS methods. This chapter concludes with self-consistent calculations of the aforementioned results.

3.1 Model

We consider a system undergoing s-wave pairing with the Zeeman field being applied in a direction that is perpendicular to the arbitrarily sized two-dimensional crystal lattice. We consider Rashba spin-orbit coupling and hopping between nearest neighbours. The tight-binding mean-field Hamiltonian is given by [28]

$$\begin{aligned}\hat{H} = &-t\sum_{<j,j'>}\sum_{\sigma}\hat{c}^{\dagger}_{j,\sigma}\hat{c}_{j',\sigma} - \mu\sum_{j}\sum_{\sigma}\hat{c}^{\dagger}_{j,\sigma}\hat{c}_{j,\sigma} \\ &- \frac{\alpha}{2}\sum_{j}\left[\left(\hat{c}^{\dagger}_{j-e_x,\downarrow}\hat{c}_{j,\uparrow} - \hat{c}^{\dagger}_{j+e_x,\downarrow}\hat{c}_{j,\uparrow}\right) + i\left(\hat{c}^{\dagger}_{j-e_y,\downarrow}\hat{c}_{j,\uparrow} - \hat{c}^{\dagger}_{j+e_y,\downarrow}\hat{c}_{j,\uparrow}\right) + h.c.\right] \\ &- h\sum_{j}\left(\hat{c}^{\dagger}_{j,\uparrow}\hat{c}_{j,\uparrow} - \hat{c}^{\dagger}_{j,\downarrow}\hat{c}_{j,\downarrow}\right) + \sum_{j}\left(\Delta\hat{c}^{\dagger}_{j,\uparrow}\hat{c}^{\dagger}_{j,\downarrow} + h.c.\right) + \sum_{j}\sum_{\sigma}V_j\hat{c}^{\dagger}_{j,\sigma}\hat{c}_{j,\sigma}, \qquad (3.1)\end{aligned}$$

where t is the hopping parameter, μ is the chemical potential, α is the Rashba spin-orbit coupling constant, h is the Zeeman field, Δ is the order parameter, V_j is the impurity potential at site j. We can consider the impurities in the system to be either none (pure superconductor), point-type, or line-type. A point-type potential is a single impurity located at a particular site of the lattice, whereas a line-type potential is a series of impurity sites configured such

that they extend over the entire $\hat{e}_y$ axis for a given $\hat{e}_x$. The first two and last two terms of Eq. 3.1 are terms that we have seen before in Eq. 2.10. The central two terms specifically deal with spin-dependent systems. The Rashba spin-orbit coupling term dictates the probability amplitude that a particle at site i hops to site j and switches its spin direction. The Zeeman field term is a simple energy-shift for particles that are aligned or anti-aligned with the externally applied magnetic field.

Provided $V_j = 0; \forall j$, and thus spatial homogeneity, Eq. 3.1 may be Fourier-transformed to provide a momentum-space representation. The momentum-space Hamiltonian is given by [19]

$$\begin{aligned}\mathcal{H} = &\sum_{\sigma} \epsilon(\mathbf{k}) \hat{c}^{\dagger}_{\mathbf{k},\sigma} \hat{c}_{\mathbf{k},\sigma} - h \sum_{\mathbf{k},\sigma,\sigma'} (\sigma_z)_{\sigma,\sigma'} \hat{c}^{\dagger}_{\mathbf{k},\sigma} \hat{c}_{\mathbf{k},\sigma'} + \alpha \sum_{\mathbf{k},\sigma,\sigma'} \mathcal{L}_0(\mathbf{k}) \cdot \sigma_{\sigma,\sigma'} \hat{c}^{\dagger}_{\mathbf{k},\sigma} \hat{c}_{\mathbf{k},\sigma'} \\ &+ \frac{1}{2} \sum_{\mathbf{k},\sigma,\sigma'} \Delta_{\sigma,\sigma'}(\mathbf{k}) \hat{c}^{\dagger}_{\mathbf{k},\sigma} \hat{c}^{\dagger}_{-\mathbf{k},\sigma'} + \frac{1}{2} \sum_{\mathbf{k},\sigma,\sigma'} \Delta^{*}_{\sigma',\sigma}(\mathbf{k}) \hat{c}_{-\mathbf{k},\sigma} \hat{c}_{\mathbf{k},\sigma'}. \end{aligned} \tag{3.2}$$

The momentum is given by $\mathbf{k} = (k_x, k_y)$, spin by σ, the energy band dispersion relation is $\epsilon(\mathbf{k}) = -2t\cos(k_x) - 2t\cos(k_y) - \mu$, the Rashba spin-orbit coupling term is $\alpha\mathcal{L}_0(\mathbf{k}) = \alpha(\sin(k_y) - \sin(k_x))$, and the gap function is given by $\Delta_{\sigma,\sigma'} = i\Delta_s(\sigma_y)_{\sigma,\sigma'}$. Stability of the superconducting state depends upon the Rashba spin-orbit coupling term being large enough to overcome the depairing effect of the Zeeman field. Diagonalization of Eq. 3.2 leads us to an analytical equation for the energy spectrum,

$$E(\mathbf{k}) = \sqrt{\epsilon(\mathbf{k})^2 + \alpha^2\mathcal{L}_0(\mathbf{k})^2 + h^2 + |\Delta(\mathbf{k})|^2 \pm 2\sqrt{\epsilon(\mathbf{k})^2\alpha^2\mathcal{L}_0(\mathbf{k})^2 + (\epsilon(\mathbf{k})^2 + |\Delta(\mathbf{k})|^2)h^2}}. \tag{3.3}$$

In order for a transition between topologically different regions to occur, the energy gap must close. The closing condition is as follows,

$$\epsilon(\mathbf{k})^2 + \alpha^2\mathcal{L}_0(\mathbf{k})^2 + h^2 + |\Delta(\mathbf{k})|^2 = 2\sqrt{\epsilon(\mathbf{k})^2\alpha^2\mathcal{L}_0(\mathbf{k})^2 + (\epsilon(\mathbf{k})^2 + |\Delta(\mathbf{k})|^2)\, h^2}. \tag{3.4}$$

h^2	$(-1)^{I_{TKNN}}$
$0 < h^2 < (4t+\mu)^2 + \Delta^2$	1
$(4t+\mu)^2 + \Delta^2 < h^2 < \mu^2 + \Delta^2$	-1
$\mu^2 + \Delta^2 < h^2 < (4t-\mu)^2 + \Delta^2$	-1
$(4t-\mu) + \Delta^2 < h^2$	1

(a) Region A: $\mu \leq -2t$

h^2	$(-1)^{I_{TKNN}}$
$0 < h^2 < \mu^2 + \Delta^2$	1
$\mu^2 + \Delta^2 < h^2 < (4t+\mu)^2 + \Delta^2$	1
$(4t+\mu)^2 + \Delta^2 < h^2 < (4t-\mu)^2 + \Delta^2$	-1
$(4t-\mu)^2 + \Delta^2 < h^2$	1

(b) Region B: $-2t < \mu \leq 0$

h^2	$(-1)^{I_{TKNN}}$
$0 < h^2 < \mu^2 + \Delta^2$	1
$\mu^2 + \Delta^2 < h^2 < (4t-\mu)^2 + \Delta^2$	1
$(4t-\mu)^2 + \Delta^2 < h^2 < (4t+\mu)^2 + \Delta^2$	-1
$(4t+\mu)^2 + \Delta^2 < h^2$	1

(c) Region C: $0 < \mu \leq 2t$

h^2	$(-1)^{I_{TKNN}}$
$0 < h^2 < (4t-\mu)^2 + \Delta^2$	1
$(4t-\mu)^2 + \Delta^2 < h^2 < \mu^2 + \Delta^2$	-1
$\mu^2 + \Delta^2 < h^2 < (4t+\mu)^2 + \Delta^2$	-1
$(4t+\mu) + \Delta^2 < h^2$	1

(d) Region D: $2t < \mu$

Table 3.1: The four unique topological regions. The first column is the inequality conditions that the Zeeman field must satisfy. The second column represents the topological phase. If 1, then the region is Abelian. If -1, then the region is non-Abelian. The first case in each region is of trivial topological phase. This table has been modified from Reference [19].

It can be shown that the closing condition is equivalent to a set of two conditions:

$$\begin{aligned} \epsilon(\mathbf{k})^2 + |\Delta(\mathbf{k})|^2 &= h^2 + \alpha^2 \mathcal{L}_0(\mathbf{k})^2 \\ |\Delta(\mathbf{k})|^2 \alpha^2 \mathcal{L}_0(\mathbf{k})^2 &= 0. \end{aligned} \tag{3.5}$$

Given s-wave pairing the only non-trivial solution to the second equation appearing in Eq. 3.5 is when $\mathcal{L}_0(k) = 0$. Hence, as per the definition of $\mathcal{L}_0(k)$, the solutions are found to be when $k = (0,0), (0,\pi), (\pi,0), (\pi,\pi)$. Armed with this knowledge, we may calculate the closing condition for each k. The solutions $k = (0,\pi)$ and $k = (\pi,0)$ are equivalent thus we are left with three unique closing conditions:

$$\begin{aligned} (4t + \mu)^2 + \Delta_s^2 &= h^2, \\ \mu^2 + \Delta_s^2 &= h^2, \\ (4t - \mu)^2 + \Delta_s^2 &= h^2. \end{aligned} \tag{3.6}$$

We wish to examine the energy spectrum utilizing Eq. 3.2 in an effort to validate the model and reproduce results as calculated in Reference [19]. The topological regions are defined by Table 3.1. Theory indicates that we should observe no zero-energy bound states with trivial solutions, an even number of zero-energy bound states if $(-1)^{I_{TKNN}} = 1$, and an odd number of zero-energy bound states when $(-1)^{I_{TKNN}} = -1$, which are are also called Majorana bound states.

3.1.1 Rashba Spin-Orbit Coupling and Zeeman Field

Consider the energy dispersion relation near the bottom of the band and neglecting the zero-point energy, $k \approx 0$, $\epsilon(\mathbf{k}) = -2t(\cos(k_x) + \cos(k_y)) \approx t(k^2 - 4)$, where $k = \sqrt{k_x^2 + k_y^2}$. We measure the energy from $-4t$, which performs a vertical shifting leaving the shape of the band structure unaltered. Thus $\epsilon(\mathbf{k}) \approx tk^2$ near the bottom of the band. Now consider the Rashba spin-orbit coupling term in the same region.

$$\alpha \mathcal{L}_0(\mathbf{k}) \cdot \sigma \approx \alpha(k_y, -k_x) \cdot \sigma, \tag{3.7}$$

where σ represent the Pauli spin matrices, $\sigma = (\sigma_x, \sigma_y, \sigma_z)$. Hence, the Rashba spin-orbit term becomes

$$i\alpha \begin{pmatrix} 0 & k_- \\ k_+ & 0 \end{pmatrix}, \tag{3.8}$$

where $k_\pm = k_x \pm ik_y$. Setting the Zeeman field to zero for the time being, we find that the dispersion relation is altered as a result of spin-orbit coupling.

$$\begin{aligned} \epsilon'_\pm(\mathbf{k}) &= \epsilon(\mathbf{k}) \pm \alpha|k| \\ &= \epsilon \pm \alpha\sqrt{\sin^2(k_x) + \sin^2(k_y)} \end{aligned} \tag{3.9}$$

We may set $k_y = 0$ (or alternatively $k_x = 0$), to obtain a cross-sectional view of the energy dispersion relation. We may later perform a solid of revolution technique to obtain a two dimensional-representation. The dispersion relation becomes

$$\epsilon(\mathbf{k}) = a(k_x \pm \frac{\alpha}{2a})^2 - \frac{\alpha^2}{4a}, \tag{3.10}$$

where a is an arbitrary positive constant. We find the normalized eigenstates to be:

$$\begin{aligned} |\psi_+\rangle &= \frac{1}{\sqrt{2}} \begin{pmatrix} 1 \\ -i\frac{k_+}{|\mathbf{k}|} \end{pmatrix} \\ |\psi_-\rangle &= \frac{1}{\sqrt{2}} \begin{pmatrix} 1 \\ i\frac{k_-}{|\mathbf{k}|} \end{pmatrix}. \end{aligned} \tag{3.11}$$

Representing $\mathbf{k}$ in polar form, $\mathbf{k} = |\mathbf{k}|e^{i\phi} = |\mathbf{k}|(\cos(\phi), \sin(\phi))$, we can find the projection of the Pauli spin matrices on these states in terms of the momentum:

$$\begin{aligned} \langle\psi_+| (\sigma_x, \sigma_y) |\psi_+\rangle &= \frac{1}{|k|}(k_y, -k_x) \\ \langle\psi_-| (\sigma_x, \sigma_y) |\psi_-\rangle &= \frac{1}{|k|}(-k_y, k_x). \end{aligned} \tag{3.12}$$

Hence the spin is orthogonal to $\mathbf{k}$, and it's direction is clockwise for the upper band when looked down from the $\hat{k}_z$, and counterclockwise for the lower band. If we examine the energy dispersion relation for $k_y = 0$, we find the structure as shown in Fig. 3.1.

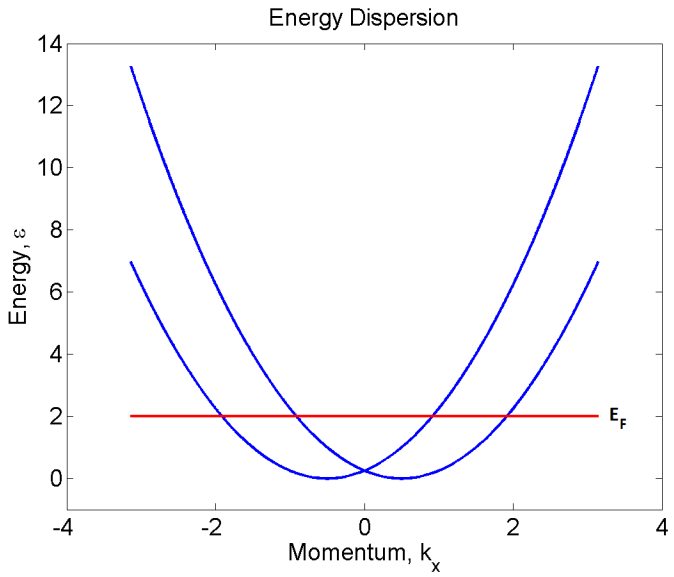

Figure 3.1: Energy dispersion relation as given in Eq. 3.10 with $a = \alpha = 1$.

If we take a solid of revolution around the Fermi level, we obtain a cross sectional view of the two unique Fermi surfaces in momentum space as depicted in Fig. 3.2.

Thus far we have treated the spin matrices, σ, as a two-dimensional vector. Thus, the spin degeneracy is preserved in $\hat{e_z}$: $\sigma_z = \pm\hbar/2$. If we now consider the case wherein the Zeeman field $h \neq 0$ we observe a vertical splitting of the bands. This is due to the electrons either aligning or anti-aligning with the direction of the Zeeman field, causing their energy to either be slightly higher or lower than in the previous example. Hence, if we place the Fermi level in the gap between these two bands, we can effectively remove the spin degree of freedom as there will exist only one Fermi surface, as illustrated in Fig. 3.3. The Fermi level only intersects one curve which produces a single Fermi surface; the outermost surface in Fig. 3.2.

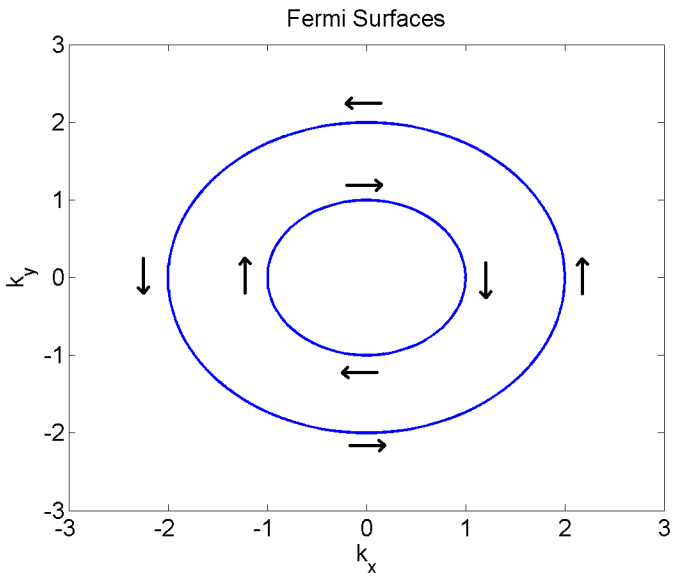

Figure 3.2: Two unique Fermi surfaces arise as a result of Rashba spin-orbit coupling. The upper and lower energy bands correspond to the inner and outer surfaces respectfully.

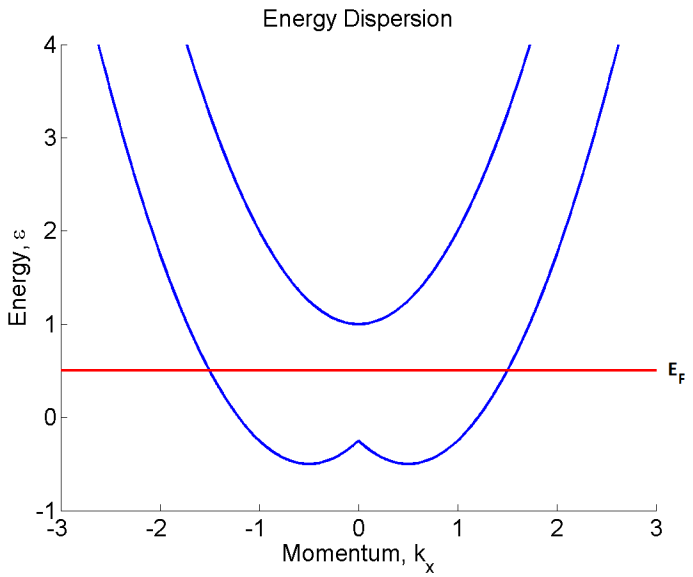

Figure 3.3: Energy dispersion relation with Zeeman field taken into account. The Fermi level, when placed in a small range, produces a single Fermi surface.

3.1.2 Preliminary Results

We examine a pure square lattice consisting of 30×30 atomic sites with s-wave pairing. We assume translational symmetry, thus performing the Fourier transform in the $\hat{e}_y$ direction, while leaving open surfaces in the $\hat{e}_x$ direction. We set the chemical potential $\mu = -1.0t$, the Rashba spin-orbit coupling constant $\alpha = 0.5t$, and the order parameter $\Delta_s = 1.0t$. We set the Zeeman field to $h = \{0.0t, 2.0t, 4.0t, 6.0t\}$, each of which corresponds to a different topological state within region B of Table 3.1. At this time we do not perform self-consistent calculations. Our results are presented in Fig. 3.5.

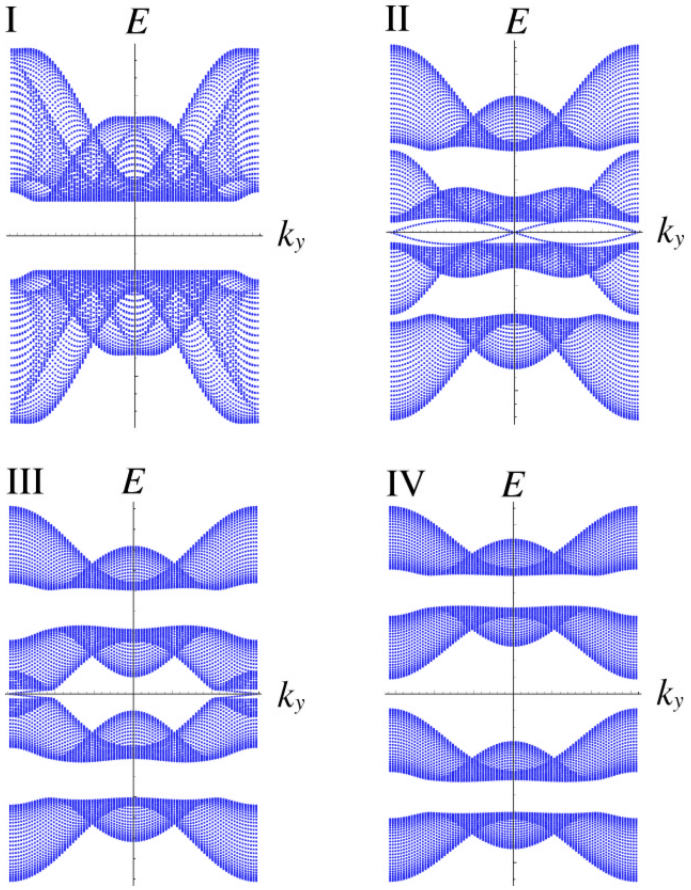

Figure 3.4: Results from reference [19]. For a 30×30 s-wave lattice with $\mu = -1.0t$, $\alpha = 0.5t$, $\Delta_s = 1.0t$, and h set to $(0t, 2t, 4t, 6t)$ corresponding to plots I - IV respectively.

Our results are in close agreement with the works of Sato, Takahashi, and Fujimoto presented in Fig. 3.4.

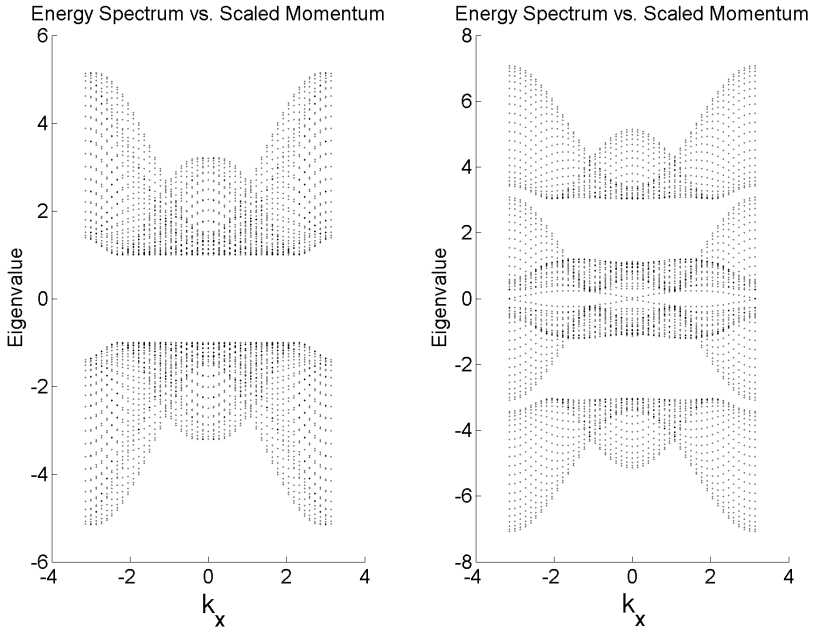

(a) $h = 0.0t$ **(b)** $h = 2.0t$

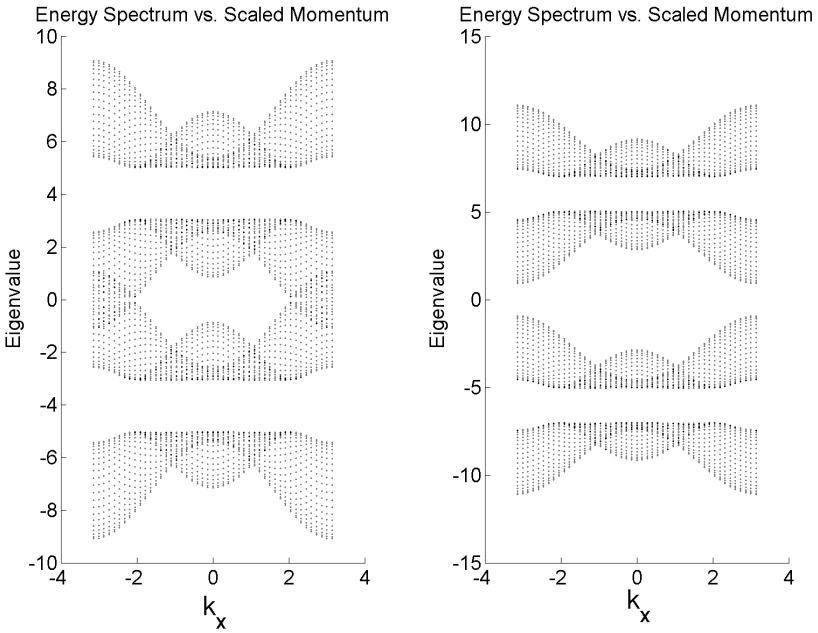

(c) $h = 4.0t$ **(d)** $h = 6.0t$

Figure 3.5: Non-self-consistent calculations of the energy spectra of the defined system. Figures 3.5b, and 3.5d have Abelian topological phases, Fig. 3.5c has non-Abelian topological phase, while Fig. 3.5a has trivial topological phase.

As per our theoretical analysis in Eq. 3.9 and Fig. 3.1, in Fig. 3.5a we notice a small horizontal shifting of the upper and lower energy bands, which is clearly visible near $k_x = 0$. As the Zeeman field is zero there is no vertical splitting of the energy bands. All other sub-figures in Figs. 3.5 and 3.4 observe splitting of the upper and lower energy bands due to the existence of the Zeeman field. That is to say, we observe an upper and lower bands for both electrons and holes hence a total of four bands appear. As per our analysis in Fig. 3.3, we notice a slight horizontal shift of the lower bands around $k_x = 0$, due to the Rashba spin-orbit coupling. The effect is most visible when $h = 2.0t$, as the Zeeman field largely dominates the Rashba term for $h \gg \alpha$.

For our non-self-consistent results it is important to note that the zero-energy bound state actually has an energy on the order of 10^{-4}, which is simply of a result of a relatively small system size. The energy quickly approaches zero as the size of the system is increased. Theory predicts the zero-energy bound state appears at the edges of the material, and hence the wavefunction should be heavily localized around the two non-periodic ends of the material.

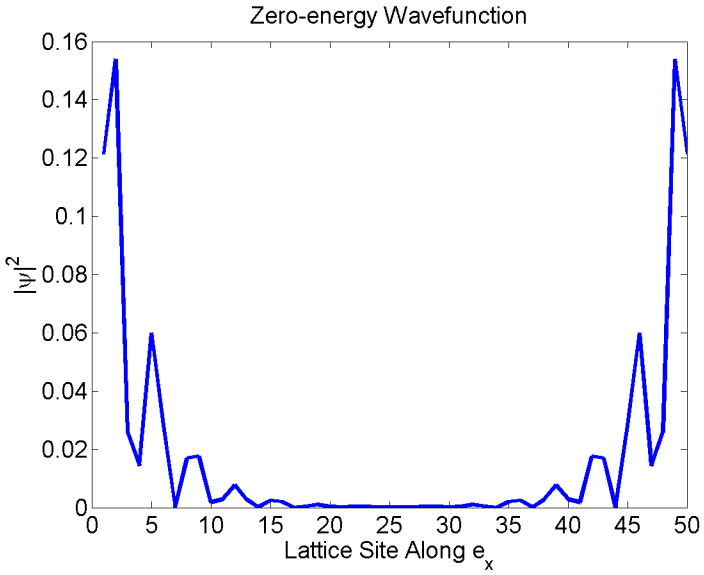

Figure 3.6: $|\psi|^2$ for the zero-energy bound state of a 50×50 lattice with $\alpha = 0.5t$, $h = 2.0t$, $\mu = -1.0t$, and $\Delta_s = 1.0t$. We see the particle is heavily localized near the edges of the lattice. The localization is the same for both spin-up and spin-down particles.

3.2 Results

3.2.1 Exploring the Parameter Space

We wish to explore various parameter sets that define each of the topological regions as presented in Table 3.1. To this end we have selected a subregion for each of the four topological regions to explore. According to our theoretical framework the order parameter is a function of the on-site pairing potential $V_{i,j}$, among other parameters. Hence, we choose a specific Zeeman field, chemical potential, and Rashba spin-orbit coupling, then self-consistently converge the order parameter. Our goal is to define a range of pairing potential strengths that allow for the system to remain in the same topological state. Our results are shown in Fig. 3.7.

3.2.2 Lowest Absolute Eigenvalue as a Function of Zeeman Field at a Given Temperature

Theory predicts that the topological phase changes from trivial to non-trivial as the Zeeman field becomes greater than some critical value. Predictions indicate that this value is given by [19] [28]:

$$h > \sqrt{(4t - \mu)^2 + \Delta^2}. \tag{3.13}$$

Under the parameter set of interest, $\mu = 3.5t$, and the initial order parameter is $\Delta = 0.35t$, $h \approx 0.61t$. The transition above this critical Zeeman field corresponds to a non-Abelian topological phase [19], this transition can be seen in Fig. 3.8.

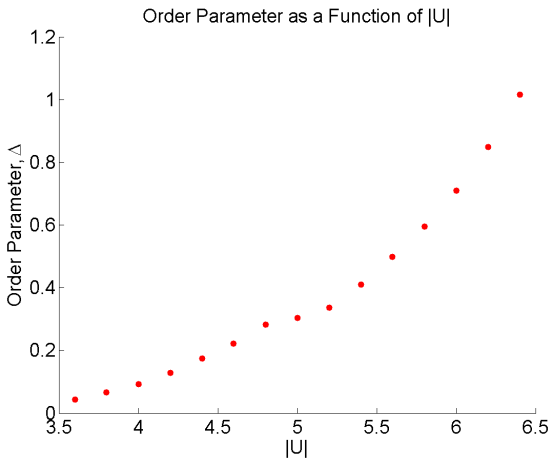

(a) Region A.2: $\mu = -3.0t$, $h = 1.5t$, $\alpha = 1.5t$, non-Abelian

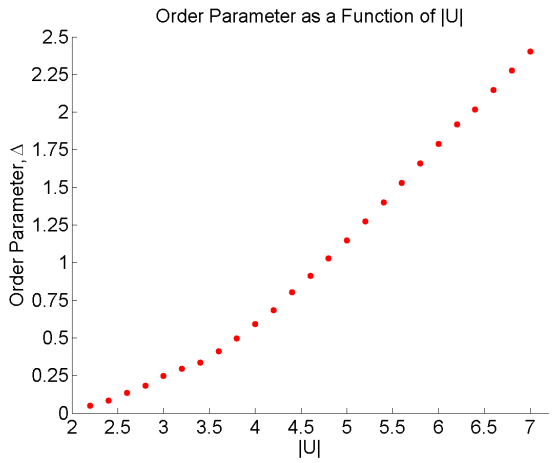

(b) Region B.1: $\mu = -1.0t$, $h = 1.0t$, $\alpha = 2.0t$, Abelian

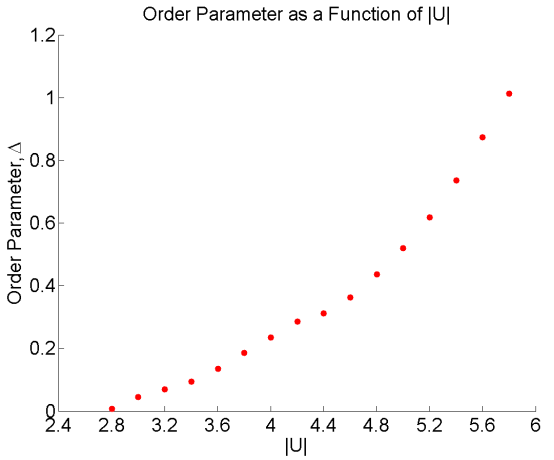

(c) Region C.2: $\mu = 1.0t$, $h = 1.5t$, $\alpha = 2.0t$, Abelian

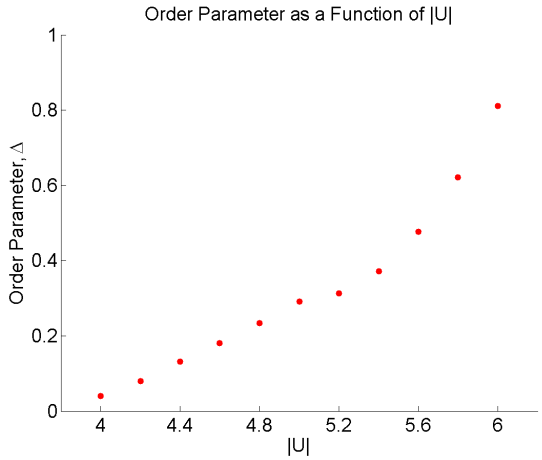

(d) Region D.2: $\mu = 3.5t$, $h = 1.0t$, $\alpha = 1.0t$, non-Abelian

Figure 3.7: The order parameter as a function of on-site pairing potential under a given set of conditions.

A minor caveat is our desire to self-consistently solve for the order parameter. The consequences of which causes the critical value to be altered slightly. These calculations were performed and their results are displayed in Fig. 3.9. Predictions become more accurate as the system size is increased. Our results predict the critical Zeeman field to lie around $h \approx 0.6t$.

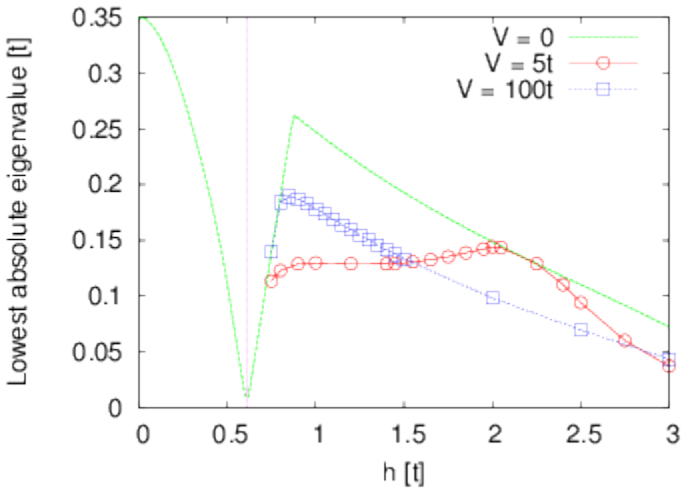

Figure 3.8: This image depicts the critical Zeeman field with $\mu = 3.50t$, $\Delta = 0.35t$. The critical value depicts where a phase transition from the trivial to non-trivial state occurs. Image from reference [28].

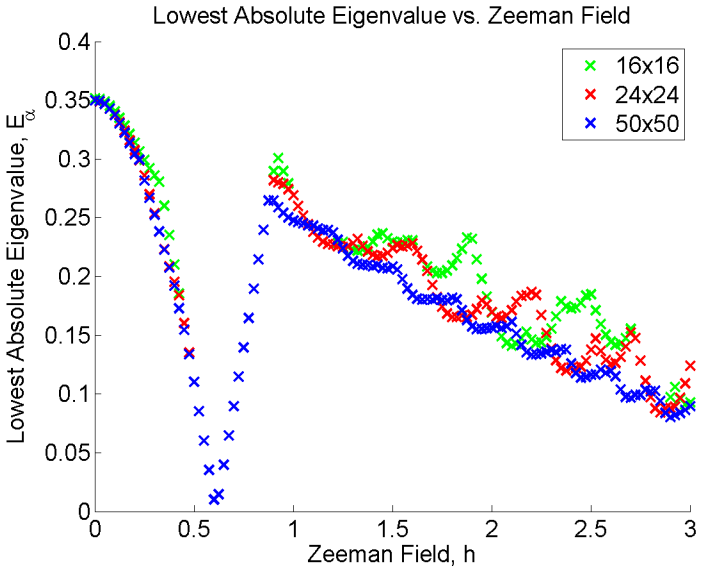

Figure 3.9: Self-consistent calculations of the critical Zeeman field under the present parameter set with zero impurities.

Our results are in close agreement with theory; providing strong evidence that there exists a transition from trivial topological phase to non-trivial topological phase as the Zeeman field is increased beyond some critical value.

3.2.3 Order Parameter as a Function of Temperature at a Given Zeeman Field

Theoretically predicting the critical temperature is of great importance. Society is engulfed in a seemingly endless journey to realize room temperature superconductors. As far as topological superconductivity and quantum computing are concerned, a higher critical temperature directly correlates to an increase in robustness. If the critical temperature is very high, micro variations of temperature provide a very small change in the overall state of the system, thus a higher degree of robustness. To this end, we theoretically predict the critical temperature of a topological superconductor under a variety of Zeeman fields. We examine a pure square lattice consisting of 40×40 atomic sites under the s-wave pairing regime. We set the chemical potential $\mu = 3.50t$, with the Zeeman field and V_j parameters set to $(h, V_j) = (1.0t, 5.6t)$ or $(h, V_j) = (2.0t, 8.0t)$.

We note that the Green-function formulation depends upon an artificial cutoff for the Matsubara frequency whereas the BdG formulation does not. As a result of the differences in formulation the two will naturally disagree unless a high enough cutoff Matsubara frequency is used in the Green-function formulation. We predict a critical temperature of $T_c \approx 0.24t$ for the parameter set as given in Fig. 3.10a, and $T_c \approx 0.21t$ for the parameter set given in Fig. 3.10b. Our results are consistent with those of Nagai *et. al* [14], indicating that the order parameter becomes more sensitive to temperature variations as the Zeeman field increases. Nagai *et. al* [14] have found that the order parameter also becomes more sensitive to non-magnetic impurities as the Zeeman field is increased.

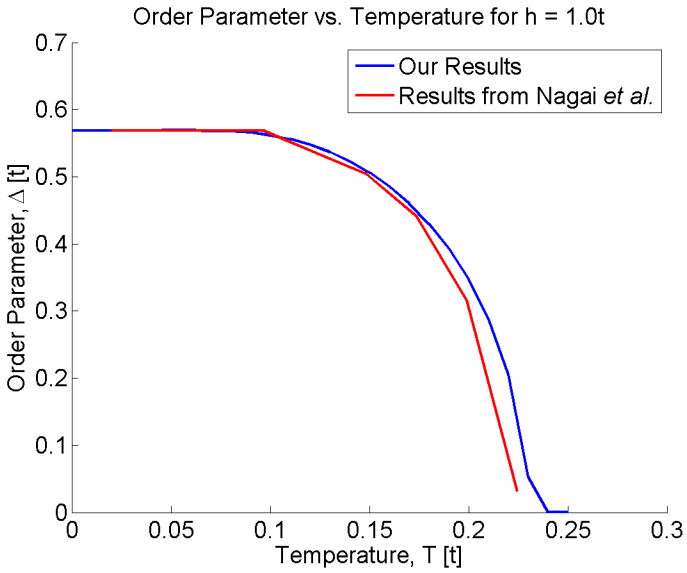

(a) $h = 1.0t$

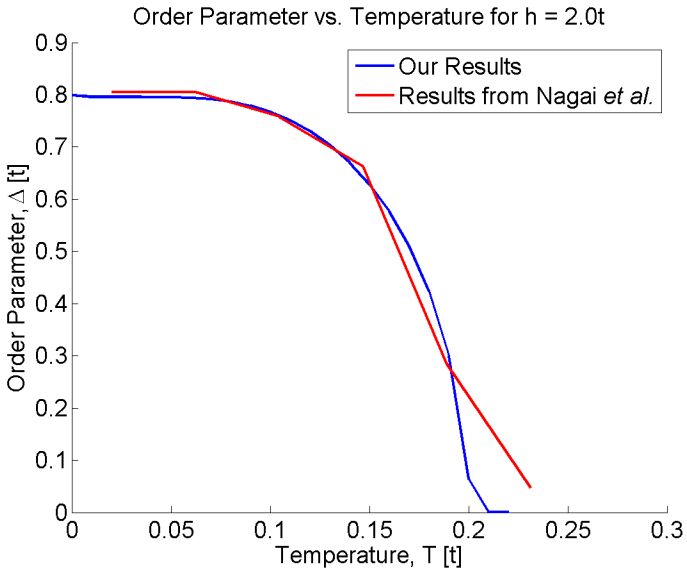

(b) $h = 2.0t$

Figure 3.10: Theoretical prediction of the critical temperature, T_c, for two different parameter sets. Results from Nagai *et. al* were obtained via private correspondence with the first author of Reference [14]; a higher Matsubara frequency was used in the presented results.

Chapter 4

Vortex Lattice

The theory presented within Section 2.2 dictates how the elements of the BdG matrix are altered in the presence of the vector potential and the resulting vortex lattice. It is useful to visualize the elements of the hopping matrix. We consider a 4×4 periodic lattice with $\frac{1}{4}$ flux quanta located at each of the four corners. We neglect the spin degree of freedom for the time being. We make reference to elements of the matrix through a block, and a location within that block. Our example lattice consists of sixteen blocks, identified by indices i_y, and i'_y.

$i_y = 0, i'_y = 0$	$i_y = 1, i'_y = 0$	$i_y = 2, i'_y = 0$	$i_y = 3, i'_y = 0$
$i_y = 0, i'_y = 1$	$i_y = 1, i'_y = 1$	$i_y = 2, i'_y = 1$	$i_y = 3, i'_y = 1$
$i_y = 0, i'_y = 2$	$i_y = 1, i'_y = 2$	$i_y = 2, i'_y = 2$	$i_y = 3, i'_y = 2$
$i_y = 0, i'_y = 3$	$i_y = 1, i'_y = 3$	$i_y = 2, i'_y = 3$	$i_y = 3, i'_y = 3$

Each of these blocks is subsequently subdivided into sixteen cells, indexed in a similar fashion through the indices i_x, and i'_x. Precisely speaking, the four vortices are at lattice sites $(i_x, i_y) = (-0.5, -0.5)$, $(3.5, -0.5)$, $(3.5, 3.5)$, and $(-0.5, 3.5)$. The upper right ($i_y = 3, i'_y = 0$), and lower left ($i_y = 0, i'_y = 3$) blocks represent periodic hopping between the top and bottom of the lattice, whereas the upper right ($i_x = 3, i'_x = 0$) and lower left ($i_x = 0, i'_x = 3$) elements of the diagonal blocks ($i_y = i'_y$) represent periodic hopping between the left and right sides of the lattice. To clarify the modifications made to the model Hamiltonian, the elements of the hopping matrix $\hat{T}$ in Eq. 2.10 are changed in accordance with the theory presented within Section 2.2. We may optionally measure lattice coordinates (i_x, i'_x, i_y, i'_y) from the centre of the lattice when computing the modified hopping elements, instead of a corner, in order to force the system into a four-fold symmetry.

4.1 Results

4.1.1 Comparison with Direct Diagonalization

To demonstrate the correctness of our implementation of the vortex lattice, we first present results for the spin-independent case. Although spin-dependent terms exist within the Hamiltonian, they are all set to zero, essentially removing the spin degree of freedom. We examine a pure 30×30 s-wave lattice with on-site pairing potential $V_{i,j} = -2.0t\delta_{i,j}$, and chemical potential $\mu = 0.0t$. We perform self-consistent calculations until suitable convergence criterion is met. We compare our results using the CKPE method to those of DD. All LDOS calculations have been performed using Eq. 2.23 with parameters $n_c = 1000$, and $\upsilon = 0.0001$.

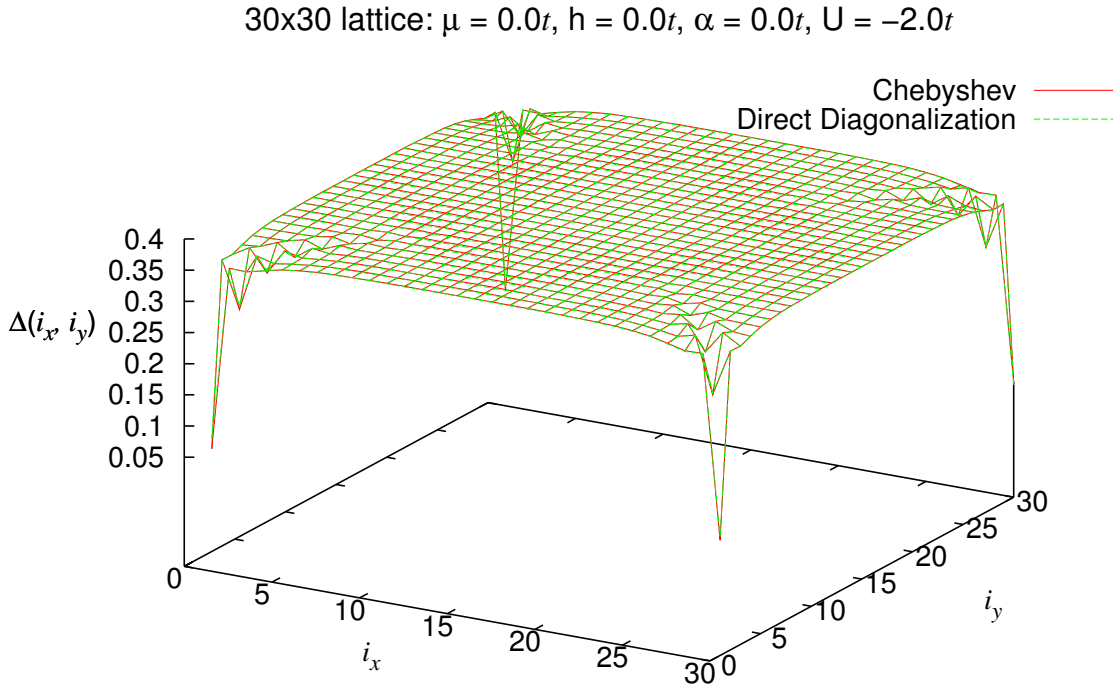

Figure 4.1: Comparison of the order parameter for CKPE and DD methods examining a conventional s-wave vortex with $\frac{1}{4}$ flux quanta located at each of the four corners.

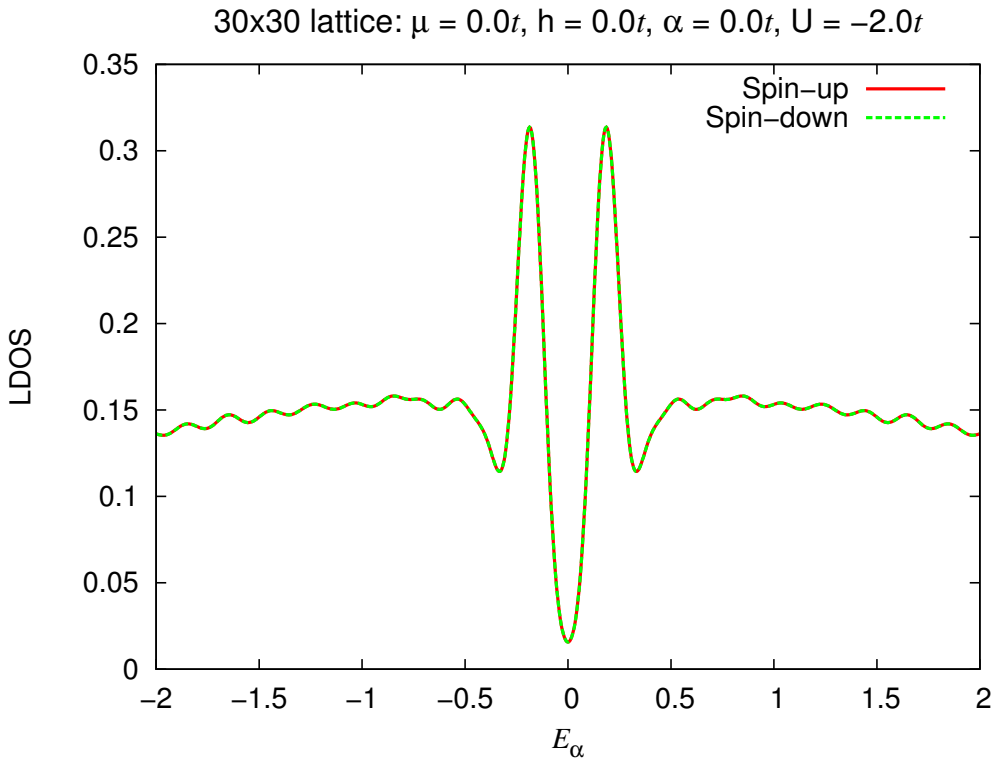

Figure 4.2: LDOS at site (0,0) for the vortex lattice presented in Fig. 4.1.

The CKPE method provides an incredibly close approximation to the results obtained through DD. As such, we conclude the CKPE method may be used as a viable substitute to efficiently compute vortex lattice solutions. As this system is of trivial topological phase, we expect no zero-energy bound states around the vortex core, which is confirmed by the LDOS at lattice site $(0, 0)$ shown in Fig. 4.2. One can see in Fig. 4.1 that the order parameter recovers to its bulk value of about 0.35 at the centre of the lattice. The bulk value is the value of the uniform order parameter when the system is uniform (i.e., without vortex or any other inhomogeneity), which shows up as the energy gap in the LDOS. In contrast, in the presence of the vortex lattice a vortex acts like a potential well for quasiparticles, so there will be bound states of quasiparticles trapped in the vortex core with energy less than the bulk energy gap. In a conventional (trivial) s-wave superconductor, however, the minimum energy

of such vortex bound states will always be finite; and the larger the bulk order parameter (the shorter the coherence length), the larger the quantization of bound-state energy levels and the higher the lowest level. For the system presented in Fig. 4.1 we find the lowest energy to be $E_\alpha = \pm 0.168t$; an order of magnitude larger than in the cases of topological superconductivity presented in Sections 4.1.4 and 4.1.3.

4.1.2 Phase Winding

The quasiparticle wavefunction, $|\psi\rangle = |\psi|e^{i\phi}$, must remain unchanged upon completion of any closed path. That is to say, the wavefunction at any point $\mathcal{A}$ must be equal to itself. Hence, $\oint_{\mathcal{C}} \nabla\phi \cdot d\mathbf{l} = \Delta\phi = 2\pi n$ for any integer n. The integer n is then equal to the number of vortices enclosed in the path $\mathcal{C}$, the sign of which implies a right or left handedness of rotation. Therefore a path enclosing a single vortex must have a phase winding of $\pm 2\pi$, which is depicted in Fig. 4.3.

4.1.3 Topological Superconductivity and Vortex Lattices

We would like to gain more insight into TSC, in particular, the properties of Majorana fermions, by creating the vortex lattice in a topological superconductor, namely if they are able to coexist. Using an extension of the data presented in Fig. 3.7, we have chosen parameter sets wherein we know TSC is capable of existing. In conjunction with this data, we have selected a few topological regions as defined in Table 3.1. The idea is to place a vortex in a system where a TSC state exists. If the resulting order parameter converges towards zero we can infer that the presence of the vortex kills TSC for that particular parameter set. If however, the order parameter converges to a finite non-zero value at all sites, that would mean that there is a vortex lattice solution. For all systems investigated we looked at a pure 41×41 s-wave lattice with spin-orbit couple and Zeeman field, and considered only nearest-neighbour hopping. Subsequent to finding at least one TSC and vortex state we wish to investigate and understand the differences between spin-up and spin-down LDOS in the vicinity of the vortex core. Theory tells us that systems with trivial topological phase will have no zero-energy states, while Abelian and non-Abelian topological phases will have an

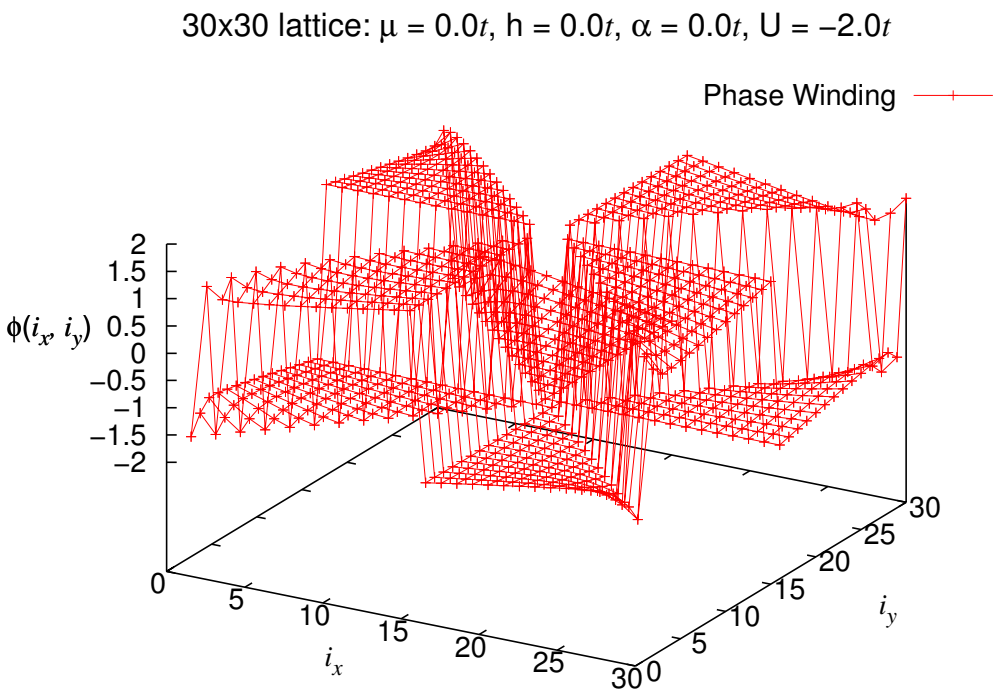

Figure 4.3: Phase of the superconducting order parameter shown in Fig. 4.1. Rotation about the vortex core leads to a $\Delta\phi = 2\pi$ phase winding.

even and odd number, respectively.

Figures 4.4a and 4.5a indicate that TSC and vortex states can coexist in both trivial and non-Abelian regimes. Through inspection of the LDOS in Fig. 4.4b we clearly see that there are no zero-energy states in the trivial phase. This is further reinforced as we found the lowest energy to be $E_\alpha = \pm 0.32415t$. Meanwhile both spin-up and spin-down LDOS in the non-Abelian topological phase shown in Fig. 4.5b exhibit a peak near zero energy. In this case the lowest energy is $E_\alpha = \pm 0.03948t$. The fact that it is not exactly zero is due to the relatively small size of the system, and precise vortex placement as mentioned above. The lowest eigenvalue is expected to approach zero for larger system size.

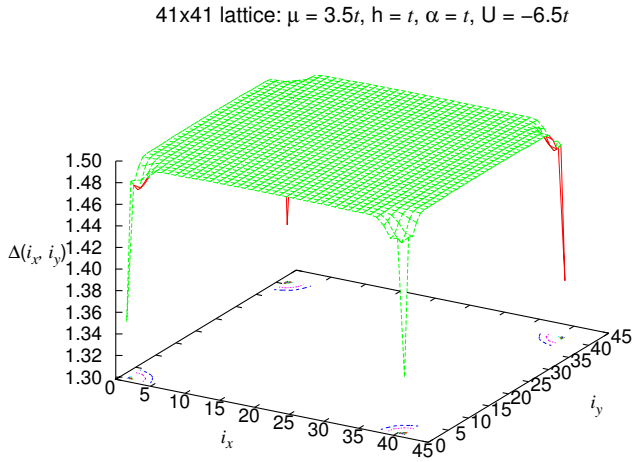

(a) Order parameter as a function of lattice position.

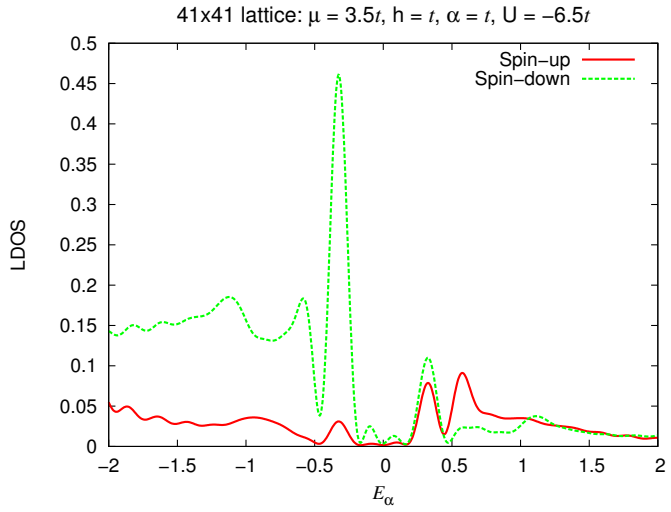

(b) Local density of states at the lattice position $(i_x, i_y) = (0, 0)$.

Figure 4.4: The bulk order parameter is $\Delta_{Bulk} \approx 1.497$, which indicates the system is in region D1 of Table 3.1, thus it is in a Trivial state.

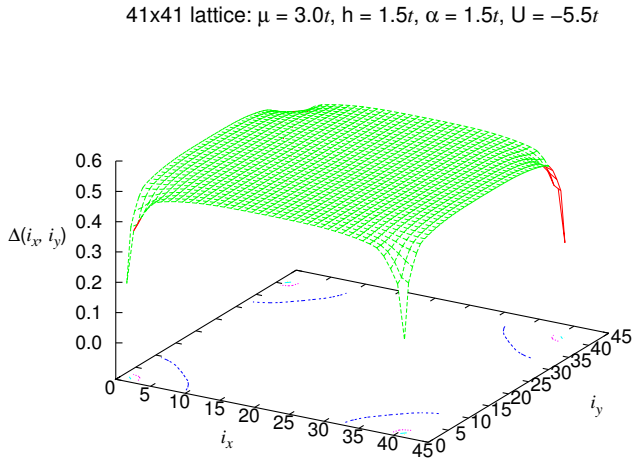

(a) Order parameter as a function of lattice position.

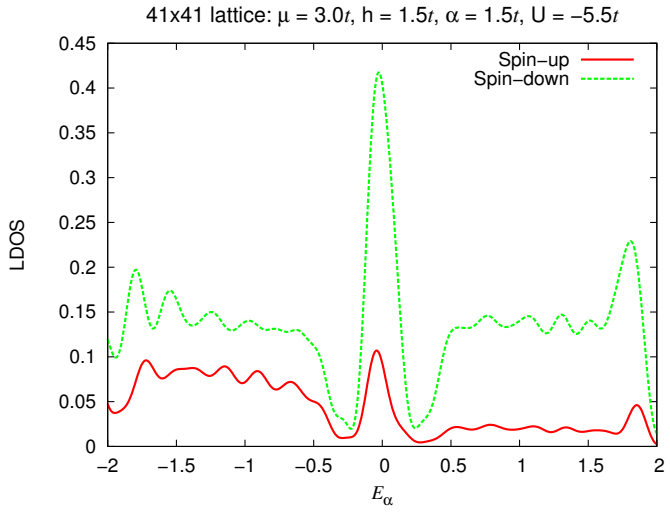

(b) Local density of states at the lattice position $(i_x, i_y) = (0, 0)$.

Figure 4.5: The bulk order parameter is $\Delta_{Bulk} \approx 0.5085$, which indicates the system is in region D2 of Table 3.1, thus it is in a non-Abelian state.

4.1.4 Comparison of High and Low Zeeman Field in Non-Abelian Vortex States

We wish to investigate how the strength of the Zeeman field affects the LDOS around the vortex core as well as in the bulk. As such we have discovered two unique states wherein TSC and vortex can coexist with non-Abelian topological phase; one with a lower Zeeman field ($h = 1.0t$), and one with a higher Zeeman field ($h = 2.0t$). Furthermore each state must have the same Rashba spin-orbit coupling constant, $\alpha = 1.0t$, and the same chemical potential, $\mu = 3.5t$, in order to provide meaningful interpretations. The pairing potential $V_{i,j} = U\delta_{i,j}$ has been chosen such that the bulk order parameters are roughly equivalent in the two systems. In Fig. 4.6 the order parameter is shown for a 24×24 system in the low Zeeman-field ($h = 1.0t, U = -5.25t$) and the high Zeeman-field ($h = 2.0t, U - 7.38t$) limit. The spin-up and spin-down LDOS are shown in Figs. 4.7a and 4.7b, respectively, comparing the two cases. The existence of vortex bound states can be seen clearly, in contrast to the LDOS in the uniform systems presented in Fig. 4.8.

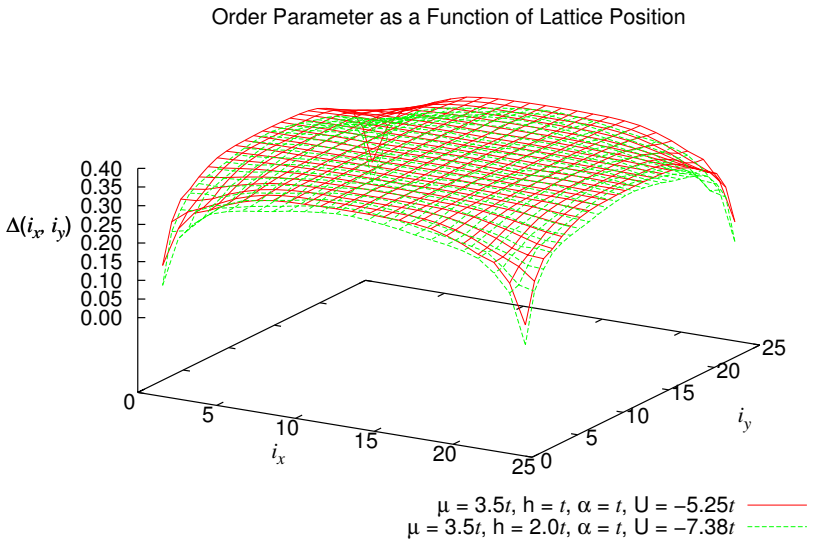

Figure 4.6: The superconducting order parameters for both non-Abelian states being examined.

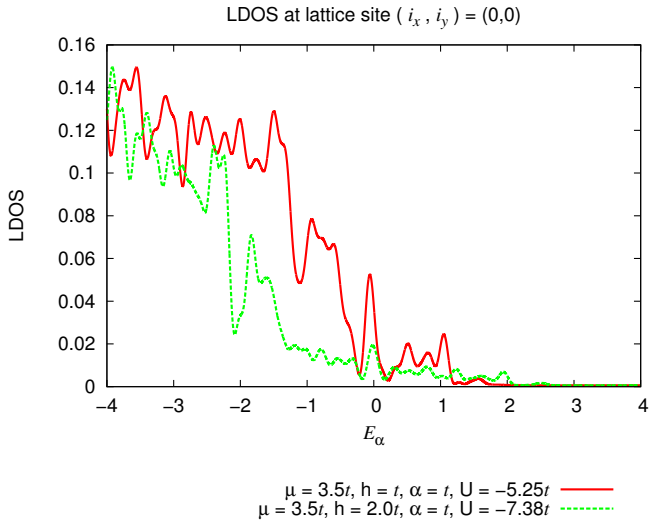

(a) Spin-up LDOS around the vortex core.

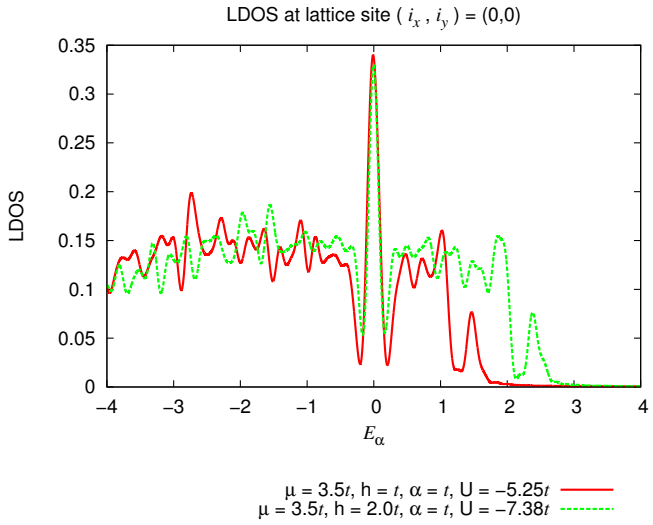

(b) Spin-down LDOS around the vortex core.

Figure 4.7: LDOS at the vortex core.

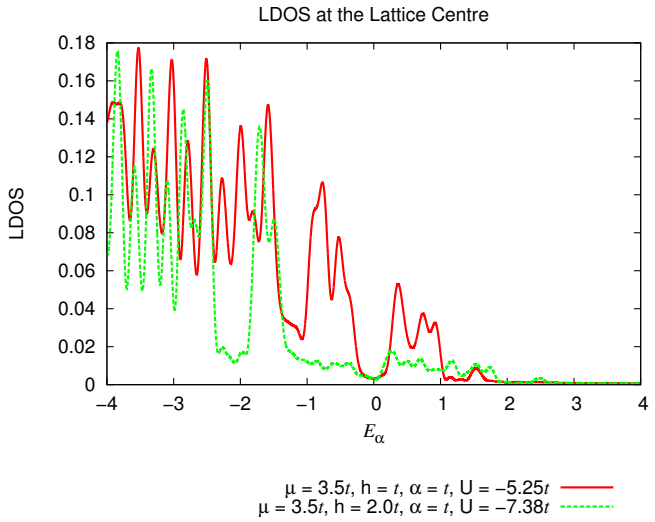

(a) Spin-up LDOS at the centre of the lattice.

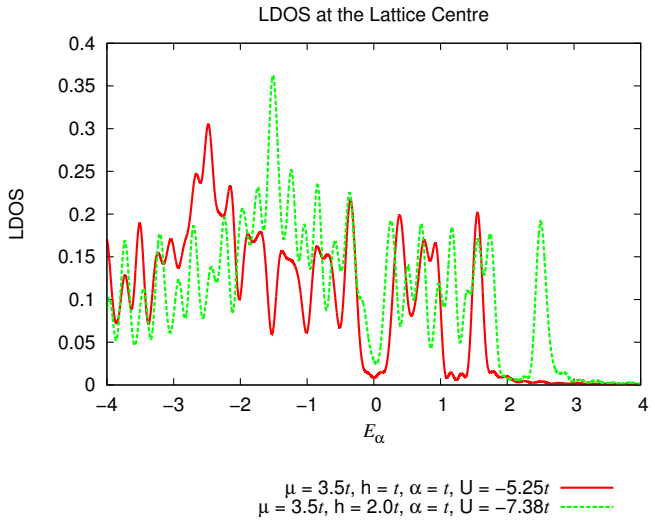

(b) Spin-down LDOS at the centre of the lattice.

Figure 4.8: LDOS at the centre of the lattice.

These figures further show that TSC and vortex states are capable of coexisting. By comparing Figs. 4.7a and 4.7b it can be seen that spin-down quasiparticles are more strongly bound to the vortex core compared to spin-up quasiparticles. These findings are consistent

with our other results presented in Fig. 4.5b. A higher Zeeman field does not change the spin-down LDOS around the vortex core too much, especially for the vortex bound states as observed in Fig. 4.7b. Meanwhile, the increased Zeeman field significantly suppresses low-energy modes of the spin-up quasiparticles around the vortex core as seen in Fig. 4.7a. By comparing Fig. 4.7a and Fig. 4.8a, or Fig. 4.7b and Fig. 4.8b, we observe the spin-up and spin-down LDOS for both high and low Zeeman field to maintain a spectral gap, with higher Zeeman field appearing to close the gap ever so slightly.

Idealistically we would expect the lowest energy level to be precisely zero; however, due to finite-size calculations, and more importantly because the vortex centre truly lies slightly outside of the lattice they are expected to be small non-zero quantities. There is $\frac{1}{4}$ flux quanta located slightly past at each of the four corners. The vortex cores are actually located at $(i_x, i_y) = \left\{(-\frac{1}{2}, -\frac{1}{2}), (-\frac{1}{2}, L_y + \frac{1}{2}), (L_x + \frac{1}{2}, -\frac{1}{2}), (L_x + \frac{1}{2}, L_y + \frac{1}{2})\right\}$. Due to the fact that we can only calculate the LDOS at lattice sites, e.g. $(i_x, i_y) = \{(0,0), (0, L_y), (L_x, 0), (L_x, L_y)\}$, we can only obtain approximations to the LDOS right at the vortex centre; a problem significantly larger lattice size would help to mitigate. Placing the vortex centres at the lattice corners would not satisfy the periodic boundary conditions. Nevertheless for low Zeeman field, $(h, V_{i,j}) = (1.0t, -5.25t\delta_{i,j})$, we find the lowest energy to be $E_\alpha = \pm 0.04722t$. With high Zeeman field, $(h, V_{i,j}) = (2.0t, -7.38t\delta_{i,j})$, we find the lowest energy to be $E_\alpha = \pm 0.03069t$.

These results suggest that a higher Zeeman field expands the vortex core such that it affects a larger area of the lattice. We may quantify this effect through analysis of how quickly the order parameter returns to the bulk value. By scaling the order parameter to unity and measuring how fast it recovers to 95% of the bulk value we find that the low Zeeman field case recovers within a radius of 5.39 sites while the high Zeeman field case recovers within a radius of 7.81 sites. As a result, if the Zeeman field is strong enough or the lattice is small enough we have a means of calculating the upper critical field, where the superconductivity is completely killed by overlap of vortices.

4.1.5 Abelian Vortex States

We would also like to qualitatively examine the differences between Abelian and non-Abelian TSC vortex states. We have found an Abelian parameter set, $\mu = 1.0t$, $\alpha = 2.0t$, $h = 1.5t$, $U = -4.5t$, such that the bulk order parameter is roughly equivalent to the non-Abelian cases presented in Section 4.1.4.

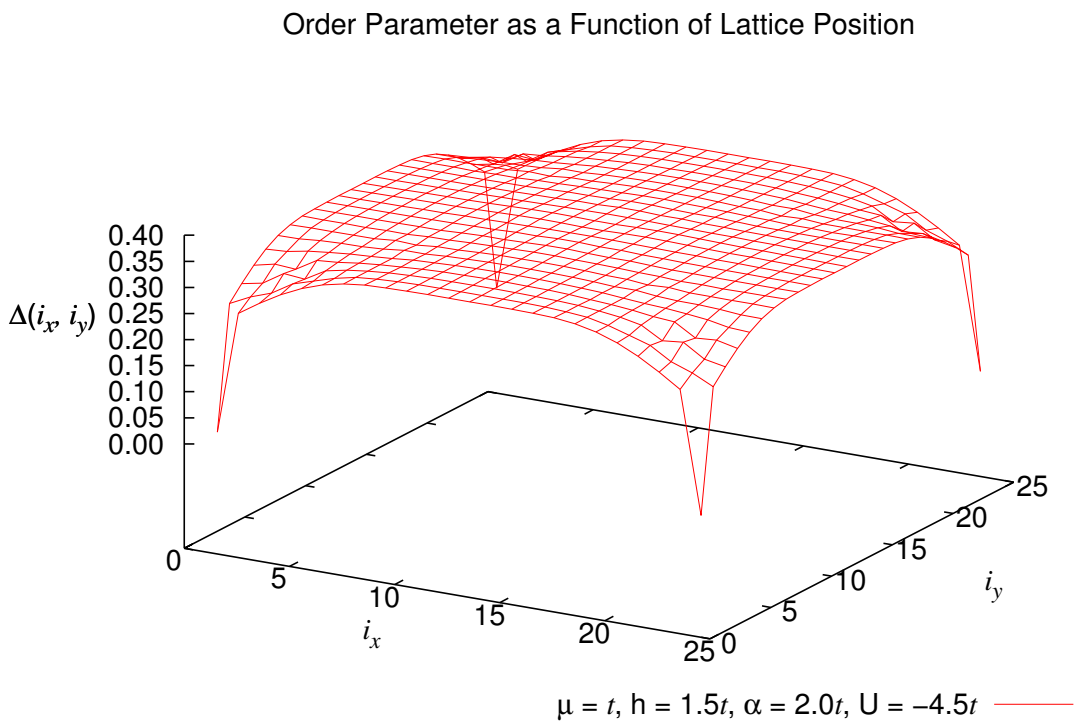

Figure 4.9: Superconducting order parameter for the Abelian case being examined.

As expected the Abelian case also contains a spectral gap in the LDOS at the lattice centre, albeit the gap is smaller than in the non-Abelian case. The spin-up and spin-down LDOS around the vortex core is heavily suppressed near zero energy as compared to the non-Abelian cases, however. We would expect the separation between the two LDOS peaks around zero energy to narrow as the system size is increased. The lowest energy calculated is $E_\alpha = \pm 0.06726t$.

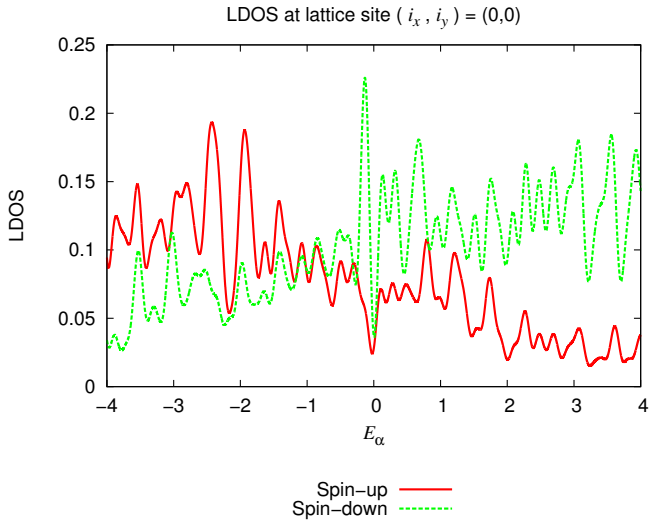

(a) LDOS at the vortex centre.

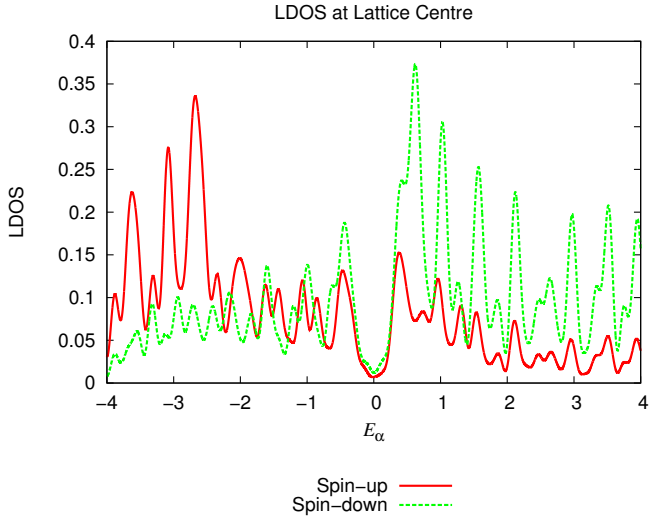

(b) LDOS at the lattice centre.

Figure 4.10: LDOS for a 24×24 lattice with $\mu = 1.0t$, $h = 1.5t$, $\alpha = 2.0t$, $U = -4.5t$.

Chapter 5

Conclusions

Inhomogeneous superconductivity has traditionally been studied through a simple direct diagonalization (DD) approach within the Bogoliubov de-Gennes' (BdG) theory. Although this method is successful in its own right it proves inadequate in the study of large-scale systems due to its computational requirements especially when particular interests are given to finding states within a specific energy range. Thus, computationally efficient algorithms must be utilized to further our understanding of superconductivity in non-uniform systems. Our methods, the Chebyshev kernel polynomial expansion (CKPE) combined with the Sakurai-Sugiura (SS) method, although much less computationally intensive than DD still require the use of large-scale parallel computing clusters for studying complex systems such as topological superconductivity. Our calculations were primarily performed on the distributed-memory cluster, Grex, at the University of Manitoba and the shared-memory cluster, Hungabee, at the University of Alberta made available through WestGrid and Compute Canada.

Due to our interests in studying Majorana bound states we first implemented the SS method. We have shown this method to be a viable, extremely efficient algorithm for computing eigenpairs within an arbitrarily defined contour for generalized eigenvalue decomposition problems. We have further shown the SS method, upon being forced to retain all eigenpair information, is equivalent to DD. The computational complexity of DD ($\mathcal{O}(n^3)$) motivated us to implemented a CKPE approach (complexity $\mathcal{O}(n^2)$) as a means to self-consistently solve for the mean fields. To further reduce computational complexity we proposed a set of transformations which permits sub-contours to be constructed. Doing so provides an additional layer of parallelism which may be exploited to enhance the computational efficiency of the SS method, particularly while utilizing the extreme computational abilities of modern day graphics processing units.

The works of Sato, Takahashi, and Fujimoto [19] showcase the differences in energy spectra and zero-energy Majoran modes of two-dimensional superconductors with varying topological phase. Trivial phase contains no zero-energy modes, Abelian phase contains an even number of zero-energy modes, while non-Abelian phase exhibits an odd number of zero-energy modes. Using our algorithms we have independently verified these findings and lent evidence to the existence of zero-energy bound states heavily localized at the free edges of topological superconductors. Nagai, Ota, and Machida [14] have shown that the critical temperature of a topological superconductor is sensitive to changes in the Zeeman field. While they used a Greens function formulation, out work has allowed for independent verification of their results within the BdG formalism.

Since they were first theorized, understanding the properties of Majorana fermions has been a goal in the field of materials science research. The ability to manipulate Majorana fermions through the use of vortices is a fundamental assumption in the use of braid theory for quantum computation. The results presented in this thesis lend evidence to the coexistence of TSC and vortex states wherein zero-energy bound states are able to exist at the vortex centre, and hence a step forth in our collective goal. We hope that our works presented in this thesis provide motivation for continued research in this exciting field of study.

Appendix A

Tweaking the Model

The electronic band structure of a two dimension lattice provides a lower bound for the parameter a. By definition $a = \frac{1}{2}(E_{max} - E_{min})$ and $b = \frac{1}{2}(E_{max} + E_{min})$, where E_{max} and E_{min} are roughly related to the electronic band structure bandwidth. According to band they, the energy as a function of momentum is given by $E(\mathbf{k}) = \epsilon + 2tcos(k_x a) + 2tcos(k_y b)$. Hence, our initial guesses were $a = 8t + 2t = 10t$ and $b = 0t$. The additional $2t$ was included in a to ensure that all possible energies are accounted for. In order to produce the simplest possible model, we decided to make use of the Dirichlet kernel. As a result of this reasoning calculations were performed using $a = \{10t, 12t, 14t, 16t\}$ with $b = 0t$. For each of these cases we decided to examine how the order parameter changes as a function of n_c. Theoretically speaking, we must keep an infinite number of terms in the Chebyshev expansion to perfectly reproduce the desired results. This condition imposes too much of a computational burden. We can however obtain reasonable results with significantly lower computational cost.

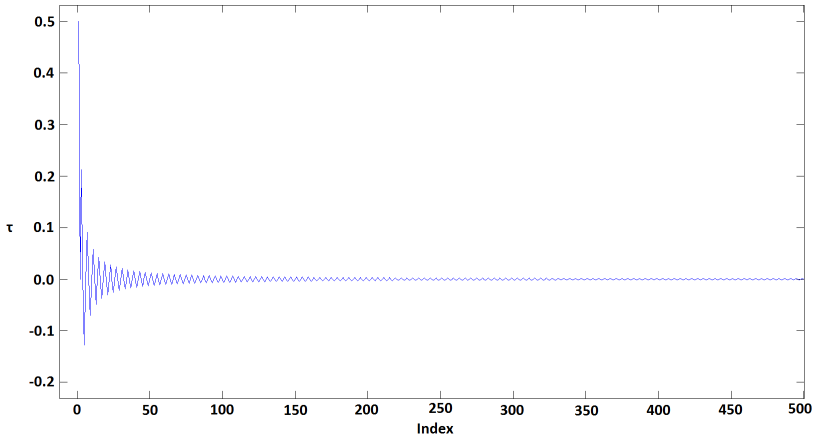

Figure A.1: The first 500 Inner product weighting factors at $T = 0t$.

The inner product weighting factors Eqs. 2.19 and 2.20 diminish quickly after the first 300 or so terms. As a result, there is not as much benefit from taking say, 3200 terms over 3000 terms. Our goal is to take the least number of terms in the Chebyshev expansion while obtaining the most accurate result.

As we may gather from Fig. A.2 and A.3, the parameter set $a = 12t$, $b = 0$, and $n_c = 800$ provides exceptional agreement with DD results while doing so within a reasonable number of terms. We next examine the effects various kernels have on the outcome given this parameter set.

The Lanczos kernel does not fit our model well at all. The sporadic behavior of the order parameter makes this kernel unfit for use. Out of the three remaining kernels, the Dirichlet simply fits the data best. Arguments can be made to use either the Fejer or Lorentz kernels, provided the number of terms is tweaked.

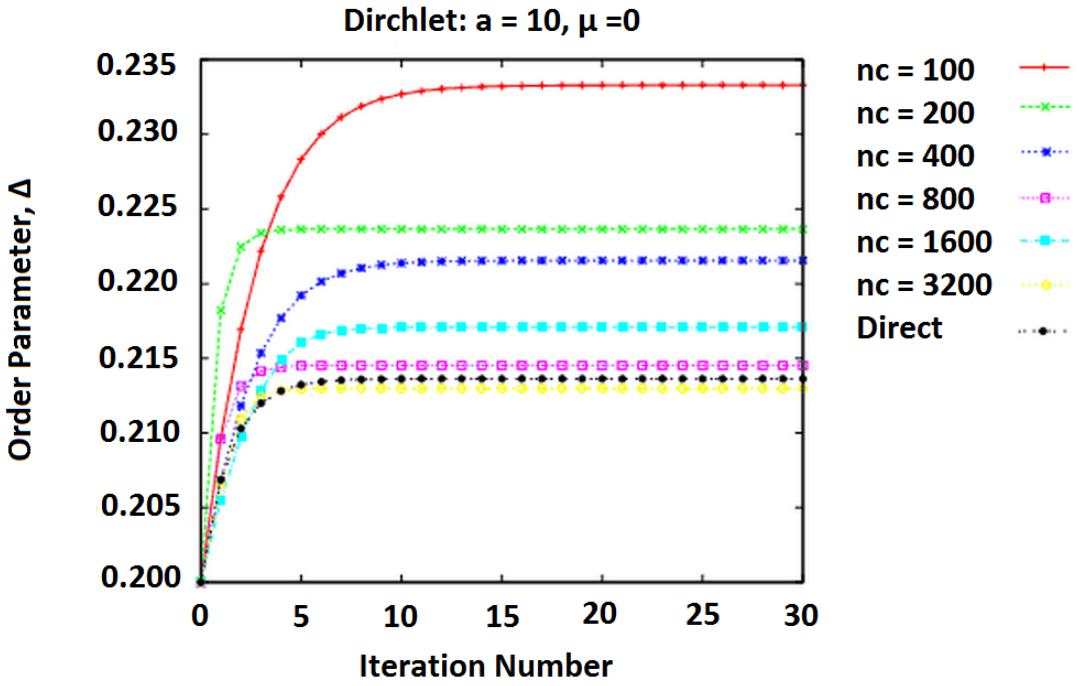

(a) $a = 10t$

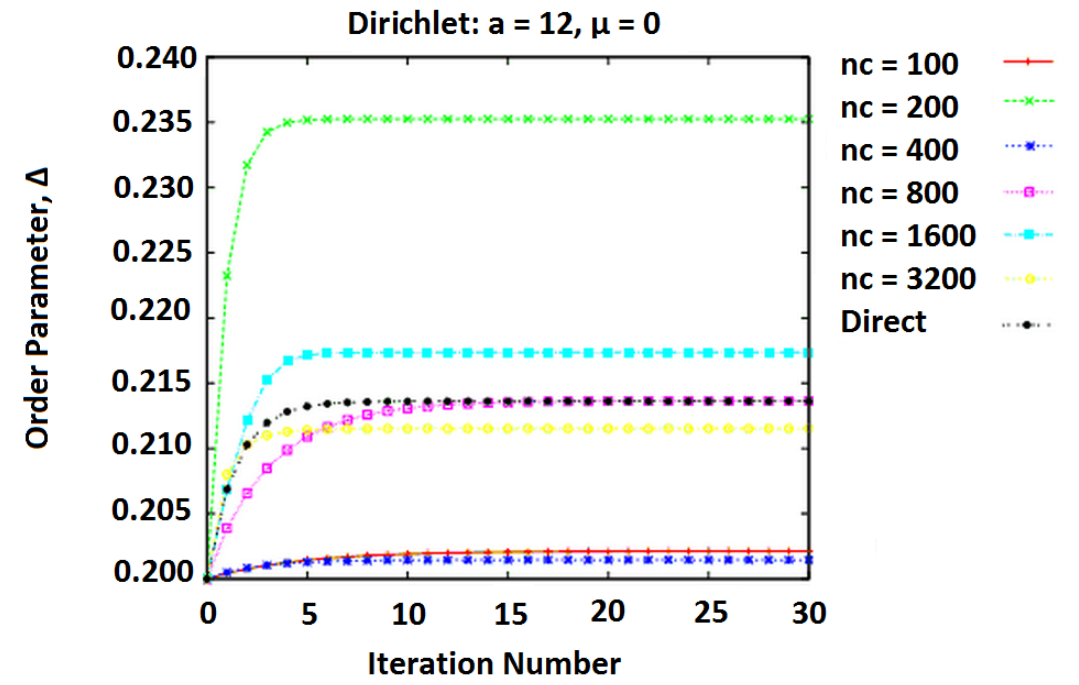

(b) $a = 12$

Figure A.2: Observing the differences between the number of terms kept within the Chebyshev expansion and the numerical factor a for the Dirichlet kernel.

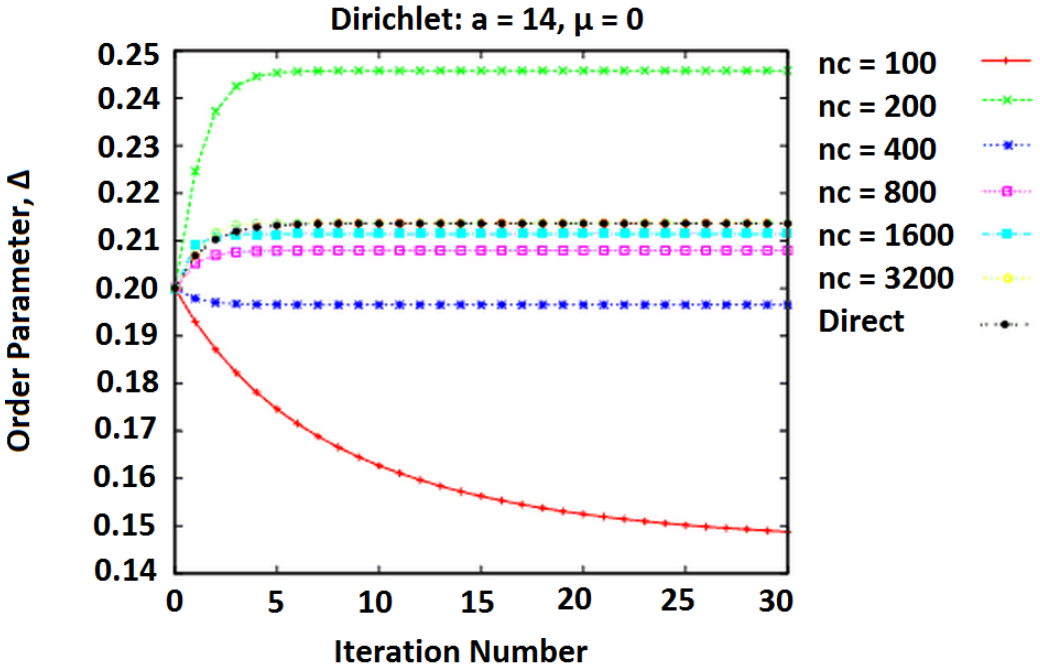

(a) $a = 14t$

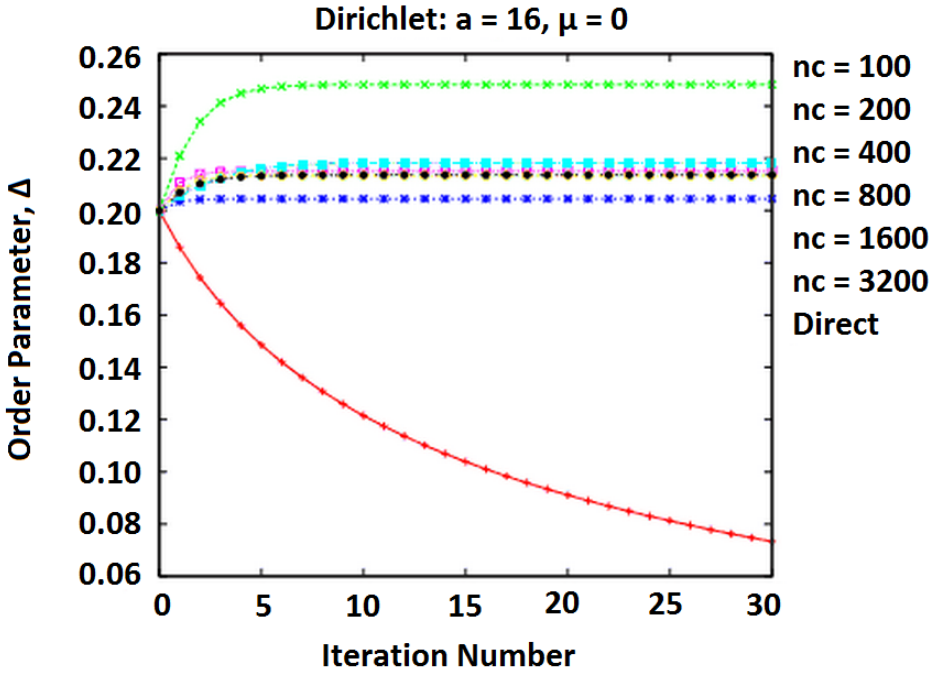

(b) $a = 16t$

Figure A.3: Observing the differences between the number of terms kept within the Chebyshev expansion and the numerical factor a for the Dirichlet kernel.

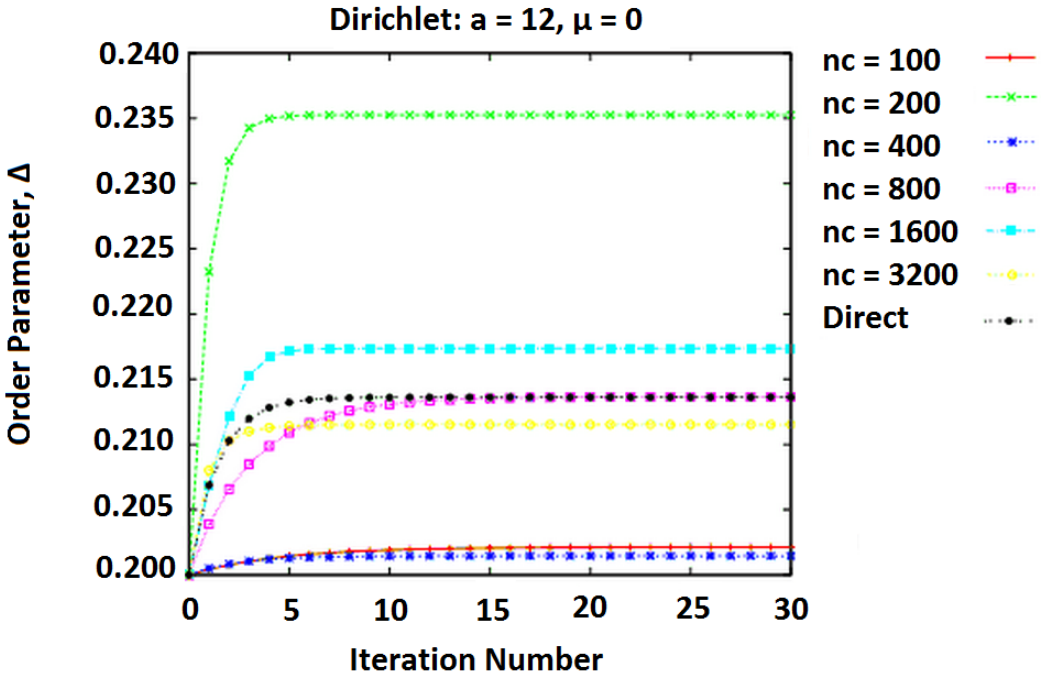

(a) Dirichlet Kernel

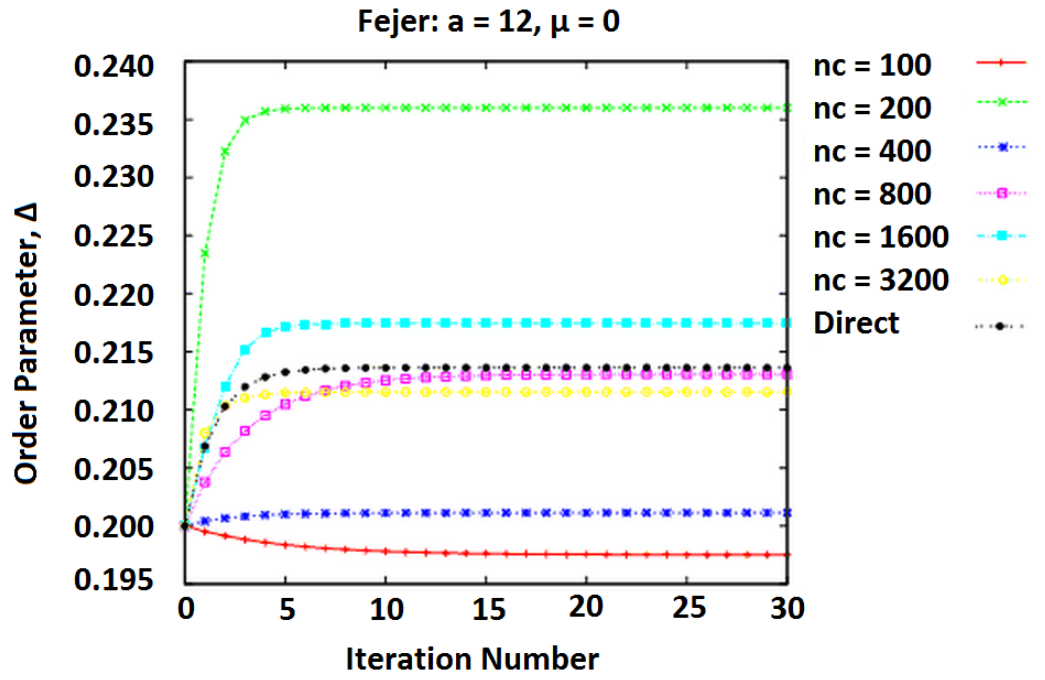

(b) Fejer Kernel

Figure A.4: Observing the differences between the Dirichlet and Fejer kernels given $a = 12t$ and $b = 0t$.

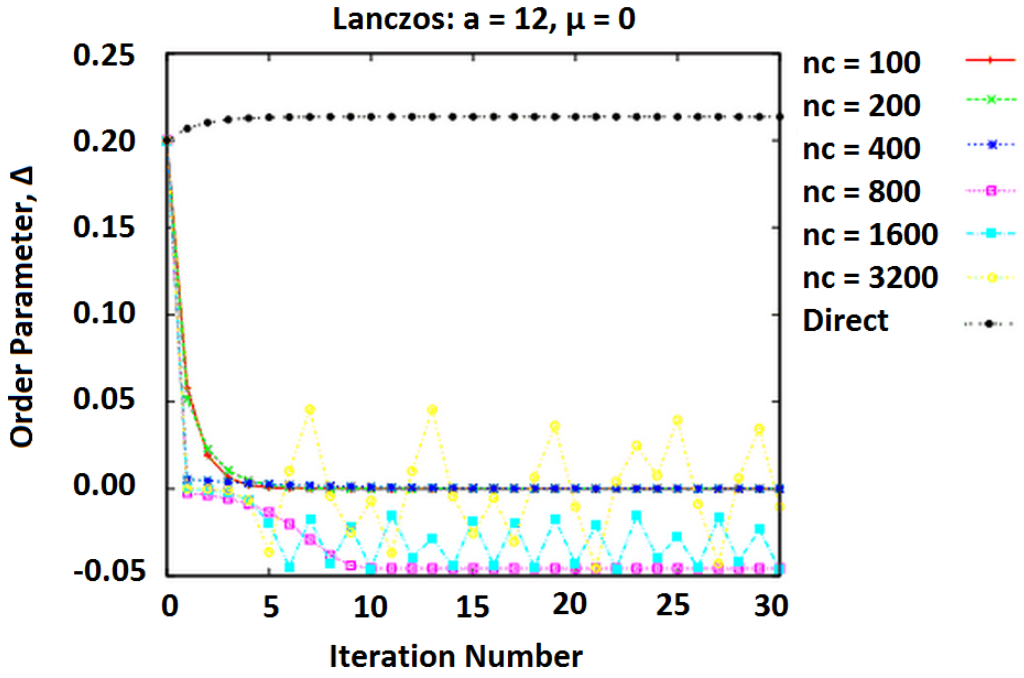

(a) Lanczos Kernel

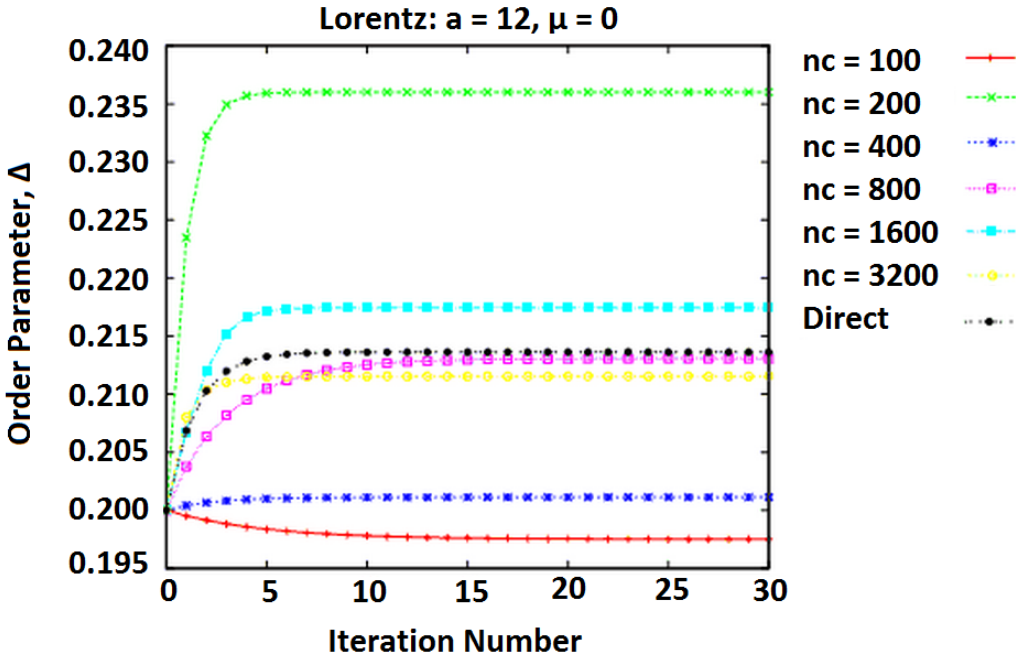

(b) Lorentz Kernel

Figure A.5: Observing the differences between the Lanczos and Lorentz kernels given $a = 12t$ and $b = 0t$.

Bibliography

[1] J. D. Guo A. Schilling, M. Cantoni and H. R. Ott. Superconductivity above 130 k in the hg-ba-ca-cu-o system. *Nature*, **363**:56, 1993.

[2] N. W. Ashcroft. Metallic hydrogen: A high-temperature superconductor? *Phys. Rev. Lett.*, **21**:21, 1968.

[3] J. Bardeen, L. N. Cooper, and J. R. Schrieffer. Theory of superconductivity. *Phys. Rev.*, **108**:1175, 1957.

[4] F. E. Camino, W. Zhou, and V. J. Goldman. Realization of a laughlin quasiparticle interferometer: Observation of fractional statistics. *Phys. Rev. B*, **72**:075342, 2005.

[5] J. Carlström, E. Babaev, and M. Speight. Type-1.5 superconductivity in multiband systems: Effects of interband couplings. *Phys. Rev. B*, **83**(17):174509, 2011.

[6] L. Covaci, F. M. Peeters, and M. Berciu. Efficient numerical approach to inhomogeneous superconductivity: The chebyshev-bogoliubov˘de gennes method. *Phys. Rev. Lett.*, **105**:167006, 2010.

[7] Dwave. The quantum computing company. `http://www.dwavesys.com/quantum-computing`.

[8] A. Yazdani et. al. Observation of majorana fermions in ferromagnetic atomic chains on a superconductor. *Science*, **346**:602, 2014.

[9] L. Fu and C. L. Kane. Superconducting proximity effect and majorana fermions at the surface of a topological insulator. *Phys. Rev. Lett.*, **100**:096407, 2008.

[10] A. Yu. Kitaev. Fault tolerant quantum computation by anyons. *Ann. Phys.*, **303**:2, 2003.

[11] F. London. On the problem of the molecular theory of superconductivity. *Phys. Rev.*, **74**:562, 1948.

[12] G. Moore and N. Read. Nonabelions in the fractional quantum hall effect. *Nuc. Phys. B*, **360**(23):362, 1991.

[13] R. H. Morf. Transition from Quantum Hall to Compressible States in the Second Landau Level: New Light on the $\nu = 5/2$ Enigma. *Phys. Rev. Lett.*, **80**:1505, 1998.

[14] Y. Nagai, Y. Ota, and M. Machida. Impurity effects in a two-dimensional topological superconductor: A link of tc robustness with a topological number. *J. Phys. Soc. Jpn.*, **83**(9):094722, 2014.

[15] C. Nayak, S. H. Simon, A. Stern, M. Freedman, and S. Das Sarma. Non-abelian anyons and topological quantum computation. *Rev. Mod. Phys.*, **80**:1083, 2008.

[16] O. X. Oskar Xaver Schlömilch, M. Witzschel, E. Cantor, R. Kahl, and C. R. Mehmke. Zeitschrift für mathematik und physik. *Druck und Verlag von B.G. Teubner*, **46**:678, 1901.

[17] J. Preskill. Topological quantum computing for beginners. page 55, 2004.

[18] E. H. Rezayi and F. D. M. Haldane. Incompressible paired hall state, stripe order, and the composite fermion liquid phase in half-filled landau levels. *Phys. Rev. Lett.*, **84**:4685, 2000.

[19] M. Sato, Y. Takahashi, and S. Fujimoto. Non-abelian topological orders and majorana fermions in spin-singlet superconductors. *Phys. Rev. B*, **82**:134521, 2010.

[20] A. Sivaguru. Majorana fermions. Master's thesis, London Imperial College, 2012.

[21] A. Stern. Non-abelian states of matter. *Nat. Phys.*, **464**:187, 2010.

[22] M. Takigawa, M. Ichioka, and K. Machida. Site-selective nuclear magnetic relaxation time in a superconducting vortex state. *J. Phys. Soc. Jpn.*, **69**(12):3943, 2000.

[23] M. Takigawa, M. Ichioka, and K. Machida. Quasiparticle structure in antiferromagnetism around the vortex and nuclear magnetic relaxation time. *J. Phys. Soc. Jpn.*, **73**(2):450, 2008.

[24] D. van Delft and P. Kes. The discovery of superconductivity. *American Institute of Physics, Phys. Today*, **S-0031-9228-1009-020-4**:38, 2010.

[25] F. Wang. Introduction to majorana fermions: Part i. ICQM and School of Physics, Peking University, 2013.

[26] F. Wilczek. Majorana returns. *Nat. Phys.*, **5**:614, 2009.

[27] Y. Ota Y. Nagai and M. Machida. Efficient numerical self-consistent mean-field approach for fermionic many-body systems by polynomial expansion on spectral density. *J. Phys. Soc. Jpn.*, **81**(2):024710, 2012.

[28] Y. Ota Y. Nagai and M. Machida. Topological s-Wave Pairing Superconductivity with Spatial Inhomogeneity: Midgap-State Appearance and Robustness of Superconductivity. *J. Phys. Soc. Jpn.*, **84**(3):034711, 2015.

Journal of the Physical Society of Japan (JPSJ)
Permission to Reproduce Figures/Tables

71-089－01

March 30, 2016

Dear Dr. Evan D. B. Smith

The Physical Society of Japan gives you permission to reproduce the material(s) you have requested.

Reproduce from:

Title: Topological s-Wave Pairing Superconductivity with Spatial Inhomogeneity: Midgap-State Appearance and Robustness of Superconductivity

Authors: Yuki Nagai, Yukihiro Ota, and Masahiko Machida

Journal of the Physical Society of Japan

Vol. 84 No. 3 (2015) Page/Article ID 034711

Material to be used: Figure 7

Reproduce to:

Title: M. Sc. Thesis, "Study of Majorana Fermions in Topological Superconductors and Vortex States Through Numerically Efficient Algorithms"

Publisher: University of Saskatchewan

Month and Year of Publication: April 2016

T. Kobayashi

Tomio Kobayashi
Chairperson of the Publication Committee of
the Physical Society of Japan

The Physical Society of Japan
5F, 2-31-22 Yushima, Bunkyo-ku, Tokyo 113-0034, JAPAN
TEL +81-3-5844-3292 FAX +81-3-5844-3290 permission@jps.or.jp

Journal of the Physical Society of Japan (JPSJ)
Permission to Reproduce Figures/Tables

71-089－02

March 30, 2016

Dear Dr. Evan D. B. Smith

The Physical Society of Japan gives you permission to reproduce the material(s) you have requested.

Reproduce from:

Title: Efficient Numerical Self-Consistent Mean-Field Approach for Fermionic Many-Body Systems by Polynomial Expansion on Spectral Density

Authors: Yuki Nagai, Yukihiro Ota, and Masahiko Machida

Journal of the Physical Society of Japan

Vol. 81 No. 2 (2012) Page/Article ID 024710

Material to be used: Figure 2

Reproduce to:

Title: M. Sc. Thesis, "Study of Majorana Fermions in Topological Superconductors and Vortex States Through Numerically Efficient Algorithms"

Publisher: University of Saskatchewan

Month and Year of Publication: April 2016

T. Kobayashi

Tomio Kobayashi
Chairperson of the Publication Committee of
the Physical Society of Japan

The Physical Society of Japan
5F, 2-31-22 Yushima, Bunkyo-ku, Tokyo 113-0034, JAPAN
TEL +81-3-5844-3292 FAX +81-3-5844-3290 permission@jps.or.jp

AMERICAN PHYSICAL SOCIETY LICENSE
TERMS AND CONDITIONS

Apr 04, 2016

This Agreement between Evan D.B. Smith ("You") and American Physical Society ("American Physical Society") consists of your license details and the terms and conditions provided by American Physical Society and Copyright Clearance Center.

License Number	3841990303614
License date	Apr 04, 2016
Licensed Content Publisher	American Physical Society
Licensed Content Publication	Physical Review B
Licensed Content Title	Non-Abelian topological orders and Majorana fermions in spin-singlet superconductors
Licensed Content Author	Masatoshi Sato, Yoshiro Takahashi, and Satoshi Fujimoto
Licensed Content Date	Oct 18, 2010
Licensed Content Volume Number	82
Type of Use	Thesis/Dissertation
Requestor type	Student
Format	Electronic
Portion	chart/graph/table/figure
Number of charts/graphs/tables/figures	1
Portion description	Figure 4
Rights for	Main product
Duration of use	Life of Current Edition
Creation of copies for the disabled	no
With minor editing privileges	no
For distribution to	Worldwide
In the following language(s)	Original language of publication
With incidental promotional use	no
The lifetime unit quantity of new product	0 to 499
The requesting person/organization is:	Evan D.B. Smith
Order reference number	None
Title of your thesis / dissertation	Study of Majorana Fermions in Topological Superconductors and Vortex States Through Numerically Efficient Algorithms
Expected completion date	Apr 2016
Expected size (number of pages)	78
Requestor Location	Evan D.B. Smith [redacted] [redacted] Attn: Evan D.B. Smith
Billing Type	Invoice
Billing Address	Evan D.B. Smith [redacted] [redacted] Attn: Evan D.B. Smith
Total	0.00 CAD
Terms and Conditions	

AMERICAN PHYSICAL SOCIETY LICENSE
TERMS AND CONDITIONS

Apr 04, 2016

This Agreement between Evan D.B. Smith ("You") and American Physical Society ("American Physical Society") consists of your license details and the terms and conditions provided by American Physical Society and Copyright Clearance Center.

License Number	3841990080374
License date	Apr 01, 2016
Licensed Content Publisher	American Physical Society
Licensed Content Publication	Physical Review B
Licensed Content Title	Non-Abelian topological orders and Majorana fermions in spin-singlet superconductors
Licensed Content Author	Masatoshi Sato, Yoshiro Takahashi, and Satoshi Fujimoto
Licensed Content Date	Oct 18, 2010
Licensed Content Volume Number	82
I would like to...	Thesis/Dissertation
Requestor type	Student
Format	Electronic
Portion	chart/graph/table/figure
Number of charts/graphs/tables/figures	1
Portion description	Table I
Rights for	Main product
Duration of use	Life of Current Edition
Creation of copies for the disabled	no
With minor editing privileges	yes
For distribution to	Worldwide
In the following language(s)	Original language of publication
With incidental promotional use	no
The lifetime unit quantity of new product	0 to 499
The requesting person/organization is:	Evan D.B. Smith
Order reference number	None
Title of your thesis / dissertation	Study of Majorana Fermions in Topological Superconductors and Vortex States Through Numerically Efficient Algorithms
Expected completion date	Apr 2016
Expected size (number of pages)	78
Requestor Location	Evan D.B. Smith [redacted] None None [redacted] Attn: Evan D.B. Smith
Billing Type	Invoice
Billing Address	Evan D.B. Smith [redacted] None None [redacted] Attn: Evan D.B. Smith
Total	0.00 CAD
Terms and Conditions	